NUMERICAL ANALYSIS OF NATURAL CONVECTIVE HEAT TRANSFER
THROUGH POROUS MEDIUM

A THESIS SUBMITTED TO
THE GRADUATE SCHOOL OF NATURAL AND APPLIED SCIENCES
OF
MIDDLE EAST TECHNICAL UNIVERSITY

BY

BENAN AYLANGAN

IN PARTIAL FULFILLMENT OF THE REQUIREMENTS
FOR
THE DEGREE OF MASTER OF SCIENCE
IN
MECHANICAL ENGINEERING

JANUARY 2006

Approval of the Graduate School of Natural and Applied Sciences

_____
Prof. Dr. Canan ÖZGEN
Director

I certify that this thesis satisfies all the requirements as a thesis for the degree of Master of Science.

_____
Prof. Dr. S. Kemal İDER
Head of Department

This is to certify that we have read this thesis and that in our opinion it is fully adequate, in scope and quality, as a thesis for the degree of Master of Science.

_____
Prof. Dr. Hafit YÜNCÜ
Supervisor

Examining Committee Members

Prof. Dr. Kazım AKYÜZLÜ   (METU, ME)   _____

Prof. Dr. Hafit YÜNCÜ   (METU, ME)   _____

Asst. Prof. Dr. İlker TARI   (METU, ME)   _____

Dr. Almıla YAZICIOĞLU   (METU, ME)   _____

Prof. Dr. M. Cevdet ÇELENLİGİL (METU, AEE)   _____

I hereby declare that all information in this document has been obtained and presented in accordance with academic rules and ethical conduct. I also declare that, as required by these rules and conduct, I have fully cited and referenced all material and results that are not original to this work.

Name, Last name : Benan AYLANGAN

Signature :

ABSTRACT

NUMERICAL ANALYSIS OF NATURAL CONVECTIVE HEAT TRANSFER THROUGH POROUS MEDIUM

Aylangan, Benan

M.S., Department of Mechanical Engineering

Supervisor: Prof. Dr. Hafit Yüncü

January 2006, 75 pages

In this thesis, natural convective heat transfer through an impermeable and fluid saturated porous medium is investigated numerically. A FORTRAN based code is developed and used in order to present the outputs of the applied model and the assumptions.

The solutions of flow fields and temperature fields are presented within the medium. Moreover, Nusselt number variations for different values of Darcy, Prandtl, and Rayleigh numbers, and some other thermodynamic properties are investigated and presented. Comparisons with previous studies are also presented.

Finally, the transition from convection to conduction in the heat transfer regime inside the porous medium is examined and an equation for estimating the heat transfer inside the porous medium is presented.

Keywords: Numerical analysis, Natural Convective, Porous media

ÖZ

GÖZENEKLİ ORTAMLARDA DOĞAL TAŞINIM İLE ISI TRANSFERİNİN SAYISAL OLARAK İNCELENMESİ

Aylangan, Benan

Yüksek Lisans Tezi, Makina Mühendisliği Anabilim Dalı

Tez Yöneticisi :   Prof. Dr. Hafit Yüncü

Ocak 2006, 75 sayfa

Bu tezde, geçirgen olmayan, akışkana doymuş gözenekli bir ortamda doğal taşınım ile ortaya çıkan ısı transferinin sayısal çözümü sunulmuştur. Uygulanan modelin sonuçlarının alınması için FORTRAN tabanlı bir bilgisayar programı kullanılmıştır.

Ortam içerisinde oluşan akışkan hareketi ve sıcaklık dağılımı grafiksel olarak sunulmuştur. Bunun yansıra Nusselt sayısının Darcy, Prandtl ve Rayleigh sayıları ve diğer termodinamik özelliklere dayalı olarak değişimi belirlenmiş ve sunulmuştur. Sonuçlar daha önce yapılmış çalışmalardan elde edilmiş sonuçlarla da karşılaştırılmıştır.

Ayrıca, gözenekli ortamdaki ısı transferinin doğal taşınımdan iletime geçiş noktası incelenmiş ve ortamdaki ısı transferini tanımlamak için bir bağıntı kurulmuş ve sunulmuştur.

Anahtar Kelimeler: Sayısal çözüm, Doğal taşınım, Gözenekli ortam

ACKNOWLEDGMENTS

I would like to express my deepest appreciation and sincere thanks to my thesis supervisor Prof. Dr. Hafit Yüncü for his guidance, suggestions, comments throughout the research.

I also would like to thank to my family for their encouragement and support through my whole educational life.

TABLE OF CONTENTS

LIST OF TABLES

TABLE

LIST OF FIGURES

FIGURES

LIST OF SYMBOLS

Abbreviations

A	aspect ratio of the medium
c_f	specific heat of the fluid (J/kg.K)
Da	Darcy number
$\vec{g}$	gravitational acceleration (m/s^2)
H	height of the control volume (m)
K	permeability of the porous medium (m^2)
k	thermal conductivity (W/m.K)
L	length (m)
m	number of nodes in the control volume in y-direction
n	number of nodes in the control volume in x-direction
P	pressure (Pa)
Pr	Prandtl number
q	heat transfer rate (W)
Ra_f	Rayleigh number of fluid
Ra_H	Rayleigh number based on height
T	Temperature (K)
T_c	cold wall temperature of control volume (K)
T_h	hot wall temperature of control volume (K)
u	x-direction component of velocity vector (m/s)
v	y-direction component of velocity vector (m/s)
$\vec{V}$	velocity vector
z	elevation (m)

Symbols

∇^2	Laplace operator
∇	gradient operator
λ	conductivity ratio
ρ	density (kg/m^3)
Δ	difference operator
μ	dynamic viscosity (Pa.s)
φ	porosity of the porous medium
ψ	streamfunction
ω	vorticity
υ	kinematic viscosity (m^2/s)
α	thermal diffusivity (m^2/s)
β	thermal expansion coefficient (K^{-1})
Δx	distance between the nodes in x-direction (m)
Δy	distance between the nodes in y-direction (m)
ΔT	$T_H - T_C$

Subscripts

f	fluid
m	medium
s	solid
w	wall
x	parameter based on length x
y	parameter based on length y
H	quantity based on height
L	quantity based on horizontal distance

Superscripts

*	dimensionless quantity

CHAPTER 1

INRODUCTION

Fluid motions due entirely to the action of a body force field such as gravitational field are usually called natural flows, in contrast to forced convection flows brought about by external agents, and the corresponding heat transfer process is termed *natural convection* or *free convection.* The movement of the fluid in natural convection, whether it is a gas or a liquid, results from the buoyancy forces imposed on the liquid when its density in the proximity of a heat transfer surface is decreased as a result of heating or increased as a result of cooling. The density difference resulting from concentration difference also gives rise to buoyancy forces due to which the flow is generated. The presence of a buoyancy force is a requirement for the existence of a natural convection flow. Ordinarily, the buoyancy arises from density differences that are the consequences of temperature or concentration gradients within the fluid. The buoyant flow arising from heat rejection to the atmosphere, heating of rooms, fire, and many other heat transfer processes, both natural and artificial, are examples of natural convection.

The term porous medium defines a material consisting of a solid matrix with an interconnected void. It is assumed that the solid matrix is either rigid (the usual situation) or it undergoes a small deformation. The interconnectedness of the void (the pores) allows the flow of one or more fluids through the material. In the simplest situation (single-phase flow) the void is saturated by a single fluid. In a natural porous medium the distribution of pores with respect to shape and size is irregular. Examples of natural porous media are beach sand, sandstone, limestone, rye bread and wood.

The research on heat transfer inside a porous medium is said to be started when Colburn [1] observed that the heat transfer rate for forced convection of air through a packed tube was greater than that of an empty tube. Following the improvements in the technologies of porous insulation, heat exchangers and filters the research on heat transfer inside porous media has gained an inevitable importance. Combarnous and Bories [2] presented a review paper on the early studies on heat transfer in porous media.

The porous medium is mainly defined by two properties; porosity and permeability. The porosity φ of a porous medium is defined as the fraction of a total volume of the medium that is occupied by void space. Thus $1-\varphi$ is the fraction that is occupied by solid. In defining φ in this way its is assumed that all the void space is connected. If in fact some of the pore space is disconnected from the remainder, then an "effective porosity" is introduced, which is defined as the ratio of connected void to total volume. For natural media, φ does not normally exceed 0.6 for beds of solid spheres of uniform diameter and φ can vary between the limits 0.2545 (rhombohedral packing) and 0.4764 (cubic packing). Nonuniformity of grain size tends to lead to smaller porosities than uniform grains, because smaller grains fill the pores formed by larger ones. For man-made materials such as metallic foams φ can approach the value 1. On the other hand, permeability is used for characterizing porous media and is defined as a length scale depending on the geometry of porous medium. Table 1.1 shows a compilation of porosities and permeability of common porous materials.

The aim of this study is to obtain the temperature and velocity fields for a determined control volume in a porous medium through the numerical solution of conservation of mass equation, conservation of momentum equation and the first law of thermodynamics (conservation of energy), and then finally to calculate Nusselt number values. The control volume is rectangular, fluid saturated porous cavity having impermeable, constant temperature vertical, and impermeable, adiabatic horizontal walls where the medium is assumed to be homogeneous and the radiation heat transfer is neglected. In this study, low Rayleigh numbers, laminar flow regime is studied; changes in the streamlines and isotherms due to the variation of Rayleigh

2

number, the effect of Rayleigh number, thermal conductivity ratio, porosity and Darcy number on the heat transfer rate are presented.

Table 1.1: Properties of common porous materials

Material	Porosity φ	Permeability K (cm²)
Black slate powder	0.57-0.66	4.9×10^{-10}-1.2×10^{-9}
Brick	0.12-0.34	4.8×10^{-11}-2.2×10^{-9}
Cigarette filters	0.17-0.49	
Coal	0.02-0.12	
Concrete (ordinary mixes)	0.02-0.07	1×10^{-9}-2.3×10^{-7}
Copper powder	0.09-0.34	3.3×10^{-6}-1.5×10^{-5}
Fiberglass	0.88-0.93	
Leather	0.56-0.59	9.5×10^{-10}-1.2×10^{-9}
Limestone	0.04-0.10	2×10^{-11}-4.5×10^{-10}
Sand	0.37-0.50	2×10^{-7}-1.8×10^{-6}
Silica powder	0.37-0.49	1.3×10^{-10}-5.1×10^{-10}
Soil	0.43-0.54	2.9×10^{-9}-1.4×10^{-7}
Spherical packing	0.36-0.43	

CHAPTER 2

LITERATURE SURVEY ON POROUS MEDIUM

2.1 Darcy Flow Model

It was 1856 that Henry Philibert Gaspard Darcy, then the "Dean of the School of Bridges and Roadways" had his report on the public fountains of Dijon, a middle size city in the central-eastern region of France, published [3]. He worked on hydraulics until his death.

Darcy's major contribution is in the area of filter hydraulics with the discovery of an empirical law that bears his name. His report on the public fountains of Dijon [3] presented the principles to follow and the formulae to use in the design and construction of water distribution systems, water filtering and the manufacturing of valves.

Having decided to investigate the phenomenon of water filtering, Darcy describes in his report a simple and ingenious apparatus. He then presents the results of carefully performed experiments done by himself and a fellow engineer in Dijon.

The experimental apparatus (Figure 2.1) used by Darcy and his colleagues was a 3.5 m high vertical column, a circular duct of interior diameter of 0.35 m, closed at the extremities with a screwed plate. Inside, at 0.20 m from the bottom, there was a horizontal separator to support the sand layer, dividing the column into two chambers. This separator was formed, from bottom to top, of an iron grid of 7 mm prismatic bars spaced by 7 mm, a grid of 5 mm cylindrical bars spaced by 5mm

(the prisms were placed perpendicular to the cylinders), and finally a metallic screen of 2 mm thickness.

In the experiment water was fed through a pipe extending from the hydraulic network of the hospital in Dijon, where his laboratory was located. The water flow rate was controlled by a valve placed along the feeding pipe connected to the top of the column.

The lower section of the column led to a one meter wide reservoir collecting the water for measuring the volumetric flow rate. The pressures above and below the sand layer were indicated via two U-shape mercury manometers equipped with diaphragms. Finally, the top chamber had an air bleeding valve for charging the column with water.

The experiments were performed with silica (quartz) sand from the Saone river, with the following composition: 58 percent of sand with grains smaller than 0.77 mm diameter, 13 percent of sand with 1.1 mm diameter grains, 12 percent of sand with 2 mm grains, and 17 percent of gravel and shell fragments of various sizes. This sand presented an average porosity of 0.38.
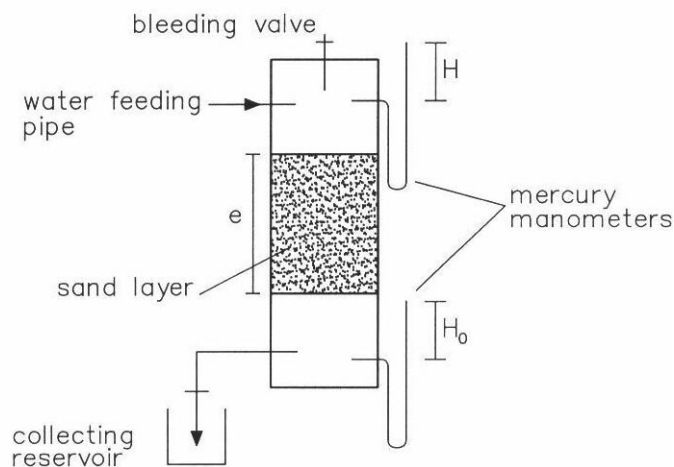
Figure 2.1:   Simple sketch of Darcy's experimental apparatus [3]

Darcy measured the flow rate by collecting a certain volume of water during a certain period of time from the lower section of the column until two consecutive measurements were equal, thus establishing a steady flow. He related the height of water inside the column via the manometer height, i.e. without visual access to the column he could predict the height of water column above the sand layer.

The experimental results were presented by Darcy in terms of volumetric flow rate and pressure difference across the sand layer. Defining a coefficient (k), now called the hydraulic conductivity, dependent on the permeability of the sand, and using the column cross-section area (s), the height of the sand layer (e), the pressure above the sand layer (P+H) (atmospheric pressure P augmented by the manometer H), and (P+H$_0$)as the pressure under the sand layer, Darcy proposed the following equation for estimating the volumetric flow rate (Q) through the column:

$$Q = \frac{ks}{e}(H + \rho g e - H_o)$$

(2.1)

or keeping the pressure under the sand layer equal to the atmospheric pressure (H$_0$=0) Equation 2.1 can be rewritten as:

$$k = U\frac{e}{\Delta P}$$

(2.2)

Darcy's Law, equation 2.1, is presently known to be limited in several aspects. It is valid, essentially, for incompressible and isothermal creeping flow (very low speed) of Newtonian fluid through a relatively long, uniform and isotropic porous medium of low hydraulic conductivity.

In his report, Darcy does not make any reference to fluid viscosity. His experiments were performed with a single fluid, namely water. With no apparent means to control the water temperature, it was impossible for Darcy to investigate fluid viscosity effects with his experimental apparatus.

Only years after the publication of the Darcy equation was the effect of fluid viscosity observed indirectly and included in Darcy's law. Hazen [4], in 1893, seems to have been the first to notice the viscosity effect in connection to the original flow equation proposed by Darcy.

$$u = (\frac{K}{\mu})(-\nabla P + \rho \vec{g}) \qquad\qquad (2.3)$$

Equation 2.3 has the hydraulic conductivity k of the original Darcy equation substituted by (K/μ). Here (∇P) is the pressure gradient in the flow direction and (μ) is the dynamic viscosity of the fluid. The coefficient (K) is independent of the nature of the fluid but it depends on the geometry of the medium. It has dimensions (length)^2 and is called the specific permeability or intrinsic permeability of the medium. In the case of single-phase flow we abbreviate this to permeability.

Henry Darcy's investigations into the hydrology of the water supply of Dijon and his experiments on steady-state unidirectional flow in a uniform medium is the only reference in the area of convectional heat transfer in a porous medium.

The Darcy's model (Hazen-Darcy model) may be generalized, as the area averaged fluid velocity through a porous medium is directly proportional to the pressure gradient in the flow direction and inversely proportional to the dynamic viscosity of the fluid saturating the porous medium.

2.2 Deterministic Models Leading to Darcy's Law

If K is determined by the geometry of the porous medium, then it may be possible to get K in terms of some geometrical parameters for simple geometry. The results on this subject are presented by Dullien [5].

For example, in the case of beds of particles or fibers we can introduce a new variable called effective average particle or fiber diameter (D_p). The hydraulic radius theory of Carman-Kozeny leads to the relationship

$$K = \frac{D^2_{p2}\varphi^3}{180(1-\varphi)^2} \qquad\qquad (2.4)$$

where

$$D_{p2} = \int_0^\infty D^3_p h(D_p)dD_p / \int_0^\infty D^2_p h(D_p)dD_p \qquad\qquad (2.5)$$

7

and h(D$_p$) is the density function for the distribution of diameters D$_p$. The constant 180 in Equation (2.4) was obtained from the best fit with experimental results. The Carman-Kozeny equation gives satisfactory results for media that consist of particles of approximately spherical shape and whose diameters fall within a narrow range. The equation is not valid in the cases of particles that deviate strongly from the spherical shape, broad particle-size distributions, and consolidated media. Nevertheless, it is widely used since it seems to be the best simple expression available.

Kozeny [6] seems to have been the pioneer in providing a physical explanation for the fluid-viscosity dependency of Darcy equation, by associating Poiseuille's theory of flow through capillaries with Darcy's empirical law of filtration. Kozeny demonstrated that by assuming uniform pressure drop and integrating Poiseuille's partial differential equation along a certain capillary length, an equation similar to the Darcy equation is obtained.

The Hagen-Poiseuille law, written as

$$\frac{s}{8\pi\mu} = U\frac{e}{\Delta P} \tag{2.6}$$

is remarkably similar to the Darcy equation: if one writes k=s/(8πμ) then equations (2.2) and (2.6) became identical. The analogy with Poiseuille flow allows the interpretation of the Darcy equation as a balance between pressure and global viscous stress, and it also supports the fluid viscosity effect on k as observed empirically by Hazen [4].

Szekely and Carr [7] studied nonisothermal gas flow through a permeable medium. The pressure variation along the medium, which is in excellent agreement with the experimental data, is obtained with an iterative scheme following an energy balance equation.

Ling and Dybbs [8] presented a numerical-theoretical investigation of the influence of temperature-dependent fluid viscosity on the steady forced convection over an isothermal flat plate bounding an infinite porous medium. Their results indicate a deviation of up to forty percent in the Nusselt number when compared with results obtained assuming uniform fluid viscosity.

Nield and Lage [9] proposed a theoretical model to account for the fluid temperature variation along the direction transverse to the flow direction, and effect of this temperature variation on the fluid viscosity, velocity, and total pressure drop.

2.3 Statistical Models Leading to Darcy's Law

Many authors have used statistical concepts in the provision of theoretical support for Darcy's law. Most authors have used constitutive assumptions in order to obtain closure of the equations, but Whitaker [10] has derived Darcy's law, for the case of incompressible fluid, without making any constitutive assumption. This theoretical development is not restricted to either homogeneous or spatially periodic porous media, but it does assume there are no abrupt changes in the structure of the medium.

If the medium has periodic structure, then the homogenization method can be used to obtain mathematically rigorous results. The method is explained in detail by Ene and Polisevski [11] and Mei [12]. Ene and Polisevski derive Darcy's law without assuming incompressibility and they go on to prove that the permeability is a symmetric positive-definite tensor.

2.4 Extensions of Darcy's Law

2.4.1 Solid Form Effect: Forchheimer's Equation

Darcy's equation is linear in the velocity. It holds when the velocity is sufficiently small. In practice, "sufficiently small" means that the Reynolds number Re_p of the flow, based on a typical pore or particle diameter, is of order unity or smaller. As velocity increases, the transition to nonlinear drag is smooth; there is no sudden transition as Reynolds number is increases from 1 to 10. This transition is not

one from laminar to turbulent since the flow in the pores is still laminar in this range of Reynolds number. However it is due to the fact that the form drag due to solid particles is now comparable with the surface drag due to friction. According to Joseph [13, 14] the appropriate modification to Darcy's equation is;

$$(\nabla P - \rho \vec{g}) = -\frac{\mu}{K} \vec{V} - c_F K^{-1/2} \rho_f |\vec{V}| \vec{V} \tag{2.7}$$

where (c_F) is a dimensionless form-drag constant. Equation (2.7) is a modification of Dupuit-Forchheiemer equation. But in fact the dependence on ($K^{-1/2} \rho_f$) is a modern discovery by Ward [15]. Ward thought that c_F might be a universal constant, with a value of approximately 0.55, but later it was found that c_F varies with the nature of the porous medium, can be as small as 0.1 in the case of foam metal fibers.

2.4.2 Flow Shear Effect: Brinkman's Equation

An alternative to Darcy's equation is what is commonly known as Brinkman's equation. This equation takes the form with inertial terms neglected;

$$(\nabla P - \rho \vec{g}) = -\frac{\mu}{K} \vec{V} + \tilde{\mu} \nabla^2 \vec{V} \tag{2.8}$$

We know have two viscous terms. The first is the usual Darcy term and the second is analogous to the Laplacian term that appears in the Navier-Stokes equation. The coefficient $\tilde{\mu}$ is an effective viscosity. Brinkman set μ and $\tilde{\mu}$ equal to each other, but in general that is not true.

In recent papers Equation (2.8) has been referred to as "Brinkman's extension of Darcy's law". Brinkman [16, 17] obtained a relationship between the permeability K and the porosity φ for an assembly of spheres as a "self-consistent" procedure, which is valid only when the porosity is sufficiently large, φ>0.6 according to Lundgren [18]. This requirement is highly restrictive since most of the practical porous media have porosities less than 0.6.

When the Brinkman equation is employed as a general momentum equation the situation is more complicated. In equation (2.8) P is the intrinsic fluid pressure, so each term in that equation represents a force per unit volume of the fluid. A

detailed averaging process leads to the result that, for an isotropic porous medium, $\tilde{\mu}/\mu = 1/\varphi T^{*}$, where T^{*} is a quantity called the tortuosity of the medium. Thus $\tilde{\mu}/\mu$ depends on the geometry of the medium.

For many practical purposes there is no need to include the Laplacian term. If it is important that a no-slip boundary condition be satisfied, then the Laplacian term is required, but its effect is significant only in a thin boundary layer whose thickness is of order $\left(\tilde{\mu} K/\mu\right)^{1/2}$, the layer being thin since the continuum hypothesis requires that $K^{1/2} \ll L$ where L is a characteristic macroscopic length scale of the problem being considered. When the Brinkman equation is employed it will usually be necessary to also account for the effects of porosity variation near the wall.

There are situations in which some authors have found it convenient to use the Brinkman equation. One such situation is to compare flows in porous media with those in clear fluids. The Brinkman equation has a parameter K (the permeability) such that the equation reduces to a form of the Navier-Stokes equation as $K/L^{2} \rightarrow \infty$ and to the Darcy equation as $K/L^{2} \rightarrow 0$.

Several recent authors have added a Laplacian term to Eqn. (2.7) to form a "Brinkman-Forchheimer" equation. The validity of this is not completely clear. As we have just seen, in order for Brinkman's equation to be valid the porosity must be large, and there is some uncertainty about the validity of the Forchheimer law at such large porosity.

2.4.3 Inertia Effect: General Equation

Vafai and Tien [19] used the volume averaging technique to solve the modified equation formed by adding the inertia, viscosity terms and the total derivative of the velocity vector to the original Darcy equation.

Vafai and Tien model is usually valid for highly permeable, high Prandtl number fluids, large pressure gradients and in the regions close to the leading edge of the boundary layer. The momentum equation of Vafai and Tien [19] is as follows:

$$\rho_f \left\langle (\vec{V} \cdot \nabla)\vec{V} \right\rangle = -\nabla\langle P \rangle + \mu_f \nabla^2 \langle \vec{V} \rangle - \frac{\mu_f \varphi}{K}\langle \vec{V} \rangle - c_F \rho_f \varphi^{3/2} \gamma (\langle \vec{V} \rangle \cdot \langle \vec{V} \rangle)\vec{J} \qquad (2.9)$$

where $\langle \vec{V} \rangle$ and $\langle P \rangle$ are the local volume averaged velocity and pressure respectively. Also γ is the porous media shape parameter.

Vafai and Tien concluded that the boundary effect is important for a very thin momentum boundary layer and it is insignificant for the overall flow consideration. But in high Prandtl number fluids and high pressure gradients, the effect of boundary is very significant as heat transfer is concerned.

Clarifying earlier work by Vafai and Tien, Hsu and Cheng [20] obtained an equation that can be written as follows:

$$\rho_f \left[\frac{1}{\varphi}\frac{\partial V}{\partial t} + \frac{1}{\varphi}\nabla \cdot \left(\frac{VV}{\varphi} \right) \right] = -\frac{1}{\varphi}\nabla(\varphi P) + \frac{\mu}{\varphi \rho_f}\nabla^2 V - \frac{\mu}{K}V - \frac{c_F \rho_f}{K^{1/2}}|V|V \qquad (2.10)$$

For an incompressible fluid, $\nabla \cdot V = 0$ and so $\varphi^{-1}\nabla \cdot (\varphi^{-1}VV)$ reduces to $\varphi^{-1}V \cdot \nabla\left(\frac{V}{\varphi} \right)$, and then Equation (2.10) becomes an easily recognizable combination of Brinkman and Forchheimer equations.

CHAPTER 3

MODELING

The main difficulty in defining a mathematical model for a porous medium is mainly due to generating a model for the conservation of momentum including all the effects. As discussed in Chapter 2, research in the porous media were limited to the Darcy equation and its extensions with the addition of the Brinkman and Forchhemier terms.

In this chapter, the most extensive and general porous media model will be presented, analyzed, and modified to a suitable form for a numerical model.

3.1 The Control Volume

As discussed earlier, in this study a numerical analysis of the flow and temperature fields of natural convection inside a porous medium is presented. Prior to examining the equations of the flow, a control volume shall be defined for which these equations will be examined.
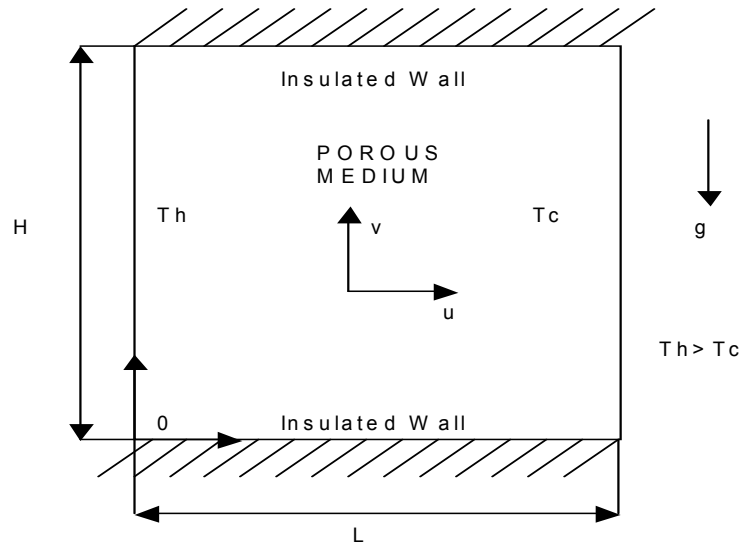
Figure 3.1:   The Control Volume

Enclosures heated from the side are most representative of porous systems that function while oriented vertically, as in the insulations for buildings, industrial cold-storage installations, and cryogenics. The model of this study to be examined is a rectangular, two-dimensional fluid saturated porous medium with length L and height H. The four walls surrounding the porous medium are impermeable and initially the fluid saturated porous layer and the four walls are isothermal and fluid inside is motionless. After a while, the left hand side and the right hand side vertical wall temperatures are changed as $T_h > T_c$. The two horizontal walls are insulated. And the third dimension is assumed to be infinitely large.

The assumptions for the control volume are that the solid matrix and fluid are locally in thermal equilibrium, and the properties are isotropic and homogeneous. Furthermore, the radiation effect of environment and internal heat generation is neglected.

14

3.2 The Conservation Equations

There are three conservation equations for a fluid in the presence of temperature gradients; the conservation of mass, the conservation of momentum and the conservation of energy. For a steady and incompressible flow these equations are as follows:

$$\nabla \cdot \vec{V} = 0 \tag{3.1}$$

$$\frac{\rho_f}{\varphi}\left[\vec{V} \cdot \nabla\right]\vec{V} = -\nabla P + \mu_f \nabla^2 \vec{V} - \frac{\rho_f c_F \varphi}{K}\left|\vec{V}\right|\vec{V} - \frac{\mu_f \varphi \vec{V}}{K} - \rho_f \beta_f \varphi(T - Tc)\vec{g} \tag{3.2}$$

$$(\rho c)_m \left[\vec{V} \cdot \nabla\right]T = k_m \nabla^2 T \tag{3.3}$$

where $\rho_f, \mu_f, \varphi, \beta_f, k_m, K, c_f, c_F$ are the fluid density, fluid dynamic viscosity, porosity of the medium, thermal expansion coefficient of the fluid, overall thermal conductivity of the medium, permeability of the medium, specific heat of the fluid and the inertial coefficient respectively. In the conservation of energy equation k_m (overall thermal conductivity of the medium), $(\rho c)_m$ (overall heat capacity per unit volume of the medium) are used. These properties are defined as:

$$k_m = (1 - \varphi)k_s + \varphi k_f \tag{3.4}$$

$$(\rho c)_m = (1 - \varphi)(\rho c)_s + \varphi(\rho c_P)_f \tag{3.5}$$

where the subscript f denotes the fluid property whereas subscript s denoting the solid matrix property.

The coefficient c_F in Equation (3.2) is related to porosity by the following equation [21].

$$c_F = \alpha \beta^{-1/2} \varphi^{-3/2} \tag{3.6}$$

Where $\alpha = 1.75$ and $\beta = 150$.

3.3 Derivation of Equations

The conservation equations are revised for the Cartesian coordinate system for two-dimensional space as follows:

15

The conservation of mass equation:

$$\frac{\partial u}{\partial x} + \frac{\partial v}{\partial y} = 0 \tag{3.7}$$

The conservation of momentum in x-direction:

$$\underbrace{\frac{\rho_f}{\varphi}\left[u\frac{\partial u}{\partial x} + v\frac{\partial u}{\partial y}\right]}_{a_1} = \underbrace{-\frac{\partial P}{\partial x}}_{a_2} + \underbrace{\mu_f\left[\frac{\partial^2 u}{\partial x^2} + \frac{\partial^2 u}{\partial y^2}\right]}_{a_3} - \underbrace{\frac{\mu_f\varphi}{K}u}_{a_4} - \underbrace{\frac{\rho_f c_F\varphi}{K^{1/2}}u\sqrt{u^2+v^2}}_{a_5} \tag{3.8}$$

The conservation of momentum in y-direction:

$$\underbrace{\frac{\rho_f}{\varphi}\left[u\frac{\partial v}{\partial x} + v\frac{\partial v}{\partial y}\right]}_{a_6} = \underbrace{-\frac{\partial P}{\partial y}}_{a_7} + \underbrace{\mu_f\left[\frac{\partial^2 v}{\partial x^2} + \frac{\partial^2 v}{\partial y^2}\right]}_{a_8} - \underbrace{\frac{\mu_f\varphi}{K}v}_{a_9} - \underbrace{\frac{\rho_f c_F\varphi}{K^{1/2}}v\sqrt{u^2+v^2}}_{a_{10}}$$

$$+\rho_f\beta_f\varphi(T-Tc)g \tag{3.9}$$

The conservation of energy equation:

$$\rho_m c_m\left[u\frac{\partial T}{\partial x} + v\frac{\partial T}{\partial y}\right] = k_m\left[\frac{\partial^2 T}{\partial x^2} + \frac{\partial^2 T}{\partial y^2}\right] \tag{3.10}$$

In order to reduce the number of unknowns, the pressure term in momentum equations can be eliminated by taking the derivatives of the momentum equation in x-direction with respect to y, and subtracting it from the derivative of the momentum equation in y-direction with respect to x. Then the equations are nondimensionalized and rewritten in terms of the stream function and vorticity which are defined as follows:

$$u = \frac{\partial \psi}{\partial y} \tag{3.11.a}$$

$$v = -\frac{\partial \psi}{\partial x} \tag{3.11.b}$$

$$\omega = \frac{\partial v}{\partial x} - \frac{\partial u}{\partial y} = -\left[\frac{\partial^2 \psi}{\partial x^2} + \frac{\partial^2 \psi}{\partial y^2}\right] \tag{3.11.c}$$

Where ψ and ω are stream function and vorticity respectively.

The nondimensional variables are:

$$\frac{uL}{v_f} = u^* \tag{3.12.a}$$

$$\frac{vL}{v_f} = v^* \tag{3.12.b}$$

16

$$\frac{x}{L} = x^*$$

(3.12.c)

$$\frac{y}{H} = y^*$$

(3.12.d)

$$\frac{\psi}{\nu_f} = \psi^*$$

(3.12.e)

$$\frac{T - T_c}{T_h - T_c} = T^*$$

(3.12.f)

$$\frac{\omega HL}{\nu_f} = \omega^*$$

(3.12.g)

3.3.1 The Momentum Equation

Taking the derivative of a_1 of Equation (3.8) with respect to y,

$$\frac{\rho_f}{\varphi}\left[\frac{\partial u}{\partial y}\cdot\frac{\partial u}{\partial x} + u\frac{\partial^2 u}{\partial y\partial x} + \frac{\partial v}{\partial y}\cdot\frac{\partial u}{\partial y} + v\frac{\partial^2 u}{\partial y^2}\right]$$

and inserting the equality from the conservation of mass equation Equation (3.7) the first degree derivatives can be easily eliminated:

$$\frac{\rho_f}{\varphi}\left[-\frac{\partial u}{\partial y}\cdot\frac{\partial v}{\partial y} + u\frac{\partial^2 u}{\partial y\partial x} + \frac{\partial v}{\partial y}\cdot\frac{\partial u}{\partial y} + v\frac{\partial^2 u}{\partial y^2}\right]$$

and the final form of the equation is:

$$\frac{\rho_f}{\varphi}\left[u\frac{\partial^2 u}{\partial y\partial x} + v\frac{\partial^2 u}{\partial y^2}\right] = \underbrace{\frac{\rho_f}{\varphi}\left[\frac{\partial \psi}{\partial y}\cdot\frac{\partial^3 \psi}{\partial y^2\partial x} - \frac{\partial \psi}{\partial x}\cdot\frac{\partial^3 \psi}{\partial y^3}\right]}_{a_{11}}$$

(3.13)

Similarly taking the derivative of a_6 of Equation (3.9) with respect to x,

$$\frac{\rho_f}{\varphi}\left[\frac{\partial u}{\partial x}\cdot\frac{\partial v}{\partial x} + v\frac{\partial^2 v}{\partial y\partial x} + \frac{\partial v}{\partial x}\cdot\frac{\partial v}{\partial y} + u\frac{\partial^2 v}{\partial x^2}\right]$$

and inserting Equation (3.7) and eliminating the first degree derivatives:

$$\frac{\rho_f}{\varphi}\left[-\frac{\partial v}{\partial y}\cdot\frac{\partial v}{\partial x} + v\frac{\partial^2 v}{\partial y\partial x} + \frac{\partial v}{\partial x}\cdot\frac{\partial v}{\partial y} + u\frac{\partial^2 v}{\partial x^2}\right]$$

resulting in the final form of the equation:

17

$$\frac{\rho_f}{\varphi}\left[v\frac{\partial^2 v}{\partial y \partial x} + u\frac{\partial^2 v}{\partial x^2}\right] = \frac{\rho_f}{\varphi}\underbrace{\left[\frac{\partial \psi}{\partial x}\cdot\frac{\partial^3 \psi}{\partial x^2 \partial y} - \frac{\partial \psi}{\partial y}\cdot\frac{\partial^3 \psi}{\partial x^3}\right]}_{a_{12}} \qquad (3.14)$$

After the derivation procedure now subtracting a_{12} of Equation (3.14) from Equation (3.13),

$$\frac{\rho_f}{\varphi}\left[\frac{\partial \psi}{\partial x}\cdot\frac{\partial^3 \psi}{\partial x^2 \partial y} - \frac{\partial \psi}{\partial y}\cdot\frac{\partial^3 \psi}{\partial x^3}\right] - \frac{\rho_f}{\varphi}\left[\frac{\partial \psi}{\partial y}\cdot\frac{\partial^3 \psi}{\partial y^2 \partial x} - \frac{\partial \psi}{\partial x}\cdot\frac{\partial^3 \psi}{\partial y^3}\right] =$$

$$\frac{\rho_f}{\varphi}\left[\frac{\partial \psi}{\partial x}\left(\frac{\partial^3 \psi}{\partial x^2 \partial y} + \frac{\partial^3 \psi}{\partial y^3}\right) - \frac{\partial \psi}{\partial y}\left(\frac{\partial^3 \psi}{\partial x^3} + \frac{\partial^3 \psi}{\partial y^2 \partial x}\right)\right] =$$

$$\frac{\rho_f}{\varphi}\left[\frac{\partial \psi}{\partial x}\cdot\frac{\partial}{\partial y}\underbrace{\left(\frac{\partial^2 \psi}{\partial x^2} + \frac{\partial^2 \psi}{\partial y^2}\right)}_{\omega} - \frac{\partial \psi}{\partial y}\cdot\frac{\partial}{\partial x}\underbrace{\left(\frac{\partial^2 \psi}{\partial x^2} + \frac{\partial^2 \psi}{\partial y^2}\right)}_{\omega}\right] =$$

$$\frac{\rho_f}{\varphi}\left[\frac{\partial \psi}{\partial y}\cdot\frac{\partial \omega}{\partial x} - \frac{\partial \psi}{\partial x}\cdot\frac{\partial \omega}{\partial y}\right] \qquad (3.15)$$

The next step is nondimensionalizing Equation (3.15) using the nondimensional variables given in Equations 3.12.a-3.12.g:

$$\frac{\rho_f}{\varphi}\left[\frac{v_f}{H}\cdot\frac{v_f}{L^2 H}\cdot\frac{\partial \psi^*}{\partial y^*}\cdot\frac{\partial \omega^*}{\partial x^*} - \frac{v_f}{L}\cdot\frac{v_f}{H^2 L}\cdot\frac{\partial \psi^*}{\partial x^*}\cdot\frac{\partial \omega^*}{\partial y^*}\right] =$$

$$\underbrace{\frac{\rho_f v_f^2}{\varphi L^2 H^2}}_{C_1^*}\underbrace{\left[\frac{\partial \psi^*}{\partial y^*}\cdot\frac{\partial \omega^*}{\partial x^*} - \frac{\partial \psi^*}{\partial x^*}\cdot\frac{\partial \omega^*}{\partial y^*}\right]}_{F_1^*}$$

Now the early equations will take a form consisting of a constant part and a functional part in terms of the variables. The nondimensional form of Equation (3.15) has a constant part C_1^* and a function part F_1^* which is a function of ω^* and ψ^*.

By using the same procedure for a_1-a_5 of Equation (3.8) and a_6-a_{10} of Equation (3.9) the final form of momentum equation in terms of stream function and vorticity can be easily obtained. And the final form will be consisting of again constants and functional parts:

$$C_1^* \cdot F_1^*(\omega^*, \psi^*) = C_2^* \cdot F_2^*(\omega^*) + C_3^* \cdot F_3^*(\omega^*) + C_4^* \cdot F_4^*(\psi^*) + C_5^* \cdot F_5^*(T^*) \qquad (3.16)$$

18

where the constant C_1^*, C_2^*, C_3^*, C_4^* and C_5^* are:

$$C_1^* = \frac{\rho_f \nu_f}{\varphi L^2 H^2}$$ (3.17.a)

$$C_2^* = \frac{\mu_f \nu_f}{L^3 H}$$ (3.17.b)

$$C_3^* = -\frac{\varphi \mu_f \nu_f}{KL\,H}$$ (3.17.c)

$$C_4^* = \frac{\rho_f \nu_f^{\,2} c_F \varphi}{L^3 K^{1/2}}$$ (3.17.d)

$$C_5^* = +\frac{\rho_f \beta_f \varphi g \Delta T}{L}$$ (3.17.e)

The remaining are the functions, which can be defined as follows:

$$F_1^*(\omega^*,\psi^*) = \frac{\partial \psi^*}{\partial y^*} \cdot \frac{\partial \omega^*}{\partial x^*} - \frac{\partial \psi^*}{\partial x^*} \cdot \frac{\partial \omega^*}{\partial y^*}$$ (3.18.a)

$$F_2^*(\omega^*) = \frac{\partial^2 \omega^*}{\partial x^{*2}} + A^2 \cdot \frac{\partial^2 \omega^*}{\partial y^{*2}}$$ (3.18.b)

$$F_3^*(\omega^*) = \omega^*$$ (3.18.c)

$$F_4^*(\psi^*) = \frac{\partial}{\partial x^*}\left[\frac{\partial \psi^*}{\partial x^*} \sqrt{\left(\frac{\partial \psi^*}{\partial x^*}\right)^2 + A^2\left(\frac{\partial \psi^*}{\partial y^*}\right)^2} \right] +$$

$$A^2 \frac{\partial}{\partial y^*}\left[\frac{\partial \psi^*}{\partial y^*} \sqrt{\left(\frac{\partial \psi^*}{\partial x^*}\right)^2 + A^2\left(\frac{\partial \psi^*}{\partial y^*}\right)^2} \right]$$ (3.18.d)

$$F_5^*(T^*) = \frac{\partial T^*}{\partial x^*}$$ (3.18.e)

where A is the aspect ratio which is defined by $A = \dfrac{L}{H}$.

Dividing both sides of the final momentum equation with C_1^* the new momentum equation takes the following form:

$$C_{1n}^* \cdot F_1^*(\omega^*,\psi^*) = C_{2n}^* \cdot F_2^*(\omega^*) + C_{3n}^* \cdot F_3^*(\omega^*) + C_{4n}^* \cdot F_4^*(\psi^*) + C_{5n}^* \cdot F_5^*(T^*)$$ (3.19)

where the constants are defined as:

$$C_{1n}^* = \frac{C_1^*}{C_1^*} = 1 \tag{3.20.a}$$

$$C_{2n}^* = \frac{C_2^*}{C_1^*} = \frac{\varphi H}{L} = \frac{\varphi}{A} \tag{3.20.b}$$

$$C_{3n}^* = \frac{C_3^*}{C_1^*} = -\frac{\varphi^2 HL}{K} = -\frac{\varphi^2}{ADa} \tag{3.20.c}$$

$$C_{4n}^* = \frac{C_4^*}{C_1^*} = \frac{\varphi^2 H^2 c_F}{L\sqrt{K}} = \frac{\varphi^2 c_F}{A^2 \sqrt{Da}} \tag{3.20.d}$$

$$C_{5n}^* = \frac{C_5^*}{C_1^*} = -\frac{\varphi^2 H^2 Lg\beta_f \Delta T}{\nu_f^2} = +\frac{\varphi^2 Ra_f}{A^2 Pr_f} \tag{3.20.e}$$

As seen from the above equations in defining the constants nondimensional numbers are introduced. These are defined as follows:

Fluid Rayleigh Number:

$$Ra_f = \frac{g\beta_f L^3 \Delta T}{\nu_f \alpha_f} \tag{3.21}$$

Rayleigh Number Based on Height:

$$Ra_H = \frac{g\beta_f HK \Delta T}{\nu_f \alpha_f} \tag{3.22}$$

Fluid Prandtl Number:

$$Pr_f = \frac{\nu_f}{\alpha_f} \tag{3.23}$$

Medium Prandtl Number:

$$Pr_m = \frac{\nu_f}{\alpha_m} \tag{3.24}$$

where $\alpha_m = \dfrac{k_m}{\rho_m c_m}$ and the conductivity ratio $\lambda = \dfrac{k_f}{k_m}$.

3.3.2 The Vorticity-Streamfunction Equation

Through the usage of streamfunctions, the conservation of mass equation is automatically satisfied and replaced by vorticity-streamfunction equation, which is defined by Equation (3.11.c) as:

$$\omega = \frac{\partial v}{\partial x} - \frac{\partial u}{\partial y} = -\left[\frac{\partial^2 \psi}{\partial x^2} + \frac{\partial^2 \psi}{\partial y^2}\right]$$

which can be nondimensionalized by using Equations (3.12.a-g) as:

$$\frac{v_f}{HL}\omega^* = -\frac{v_f}{L^2}\frac{\partial^2 \psi^*}{\partial x^{*2}} - \frac{v_f}{H^2}\frac{\partial^2 \psi^*}{\partial y^{*2}} \quad \text{from which } \omega^* \text{ can easily be defined as:}$$

$$\omega^* = -\frac{1}{A}\frac{\partial^2 \psi^*}{\partial x^{*2}} - A\frac{\partial^2 \psi^*}{\partial y^{*2}} \tag{3.25}$$

3.3.3 The Energy Equation

Again using the nondimensional numbers and starting from Equation (3.10) the energy equation becomes:

$$\rho_m c_m \left[\frac{\partial \psi}{\partial y}\frac{\partial T}{\partial x} - \frac{\partial \psi}{\partial x}\frac{\partial T}{\partial y}\right] = k_m \left[\frac{\partial^2 T}{\partial x^2} + \frac{\partial^2 T}{\partial y^2}\right] \tag{3.26.a}$$

$$\rho_m c_m \left[\frac{v_f}{H}\frac{\Delta T}{L}\frac{\partial \psi^*}{\partial y^*}\frac{\partial T^*}{\partial x^*} - \frac{v_f}{L}\frac{\Delta T}{H}\frac{\partial \psi^*}{\partial x^*}\frac{\partial T^*}{\partial y^*}\right] = k_m \left[\frac{\Delta T}{L^2}\frac{\partial^2 T^*}{\partial x^{*2}} + \frac{\Delta T}{H^2}\frac{\partial^2 T^*}{\partial y^{*2}}\right] \tag{3.26.b}$$

$$Pr_m \left[\frac{\partial \psi^*}{\partial y^*}\frac{\partial T^*}{\partial x^*} - \frac{\partial \psi^*}{\partial x^*}\frac{\partial T^*}{\partial y^*}\right] = \frac{1}{A}\frac{\partial^2 T^*}{\partial x^{*2}} + A\frac{\partial^2 T^*}{\partial y^{*2}} \tag{3.26.c}$$

3.4 Boundary Conditions

After the nondimensionalizing procedure of the equations now the boundary conditions of the control volume must be presented.

For x=0:

$$x^* = 0 , \ u^* = 0 , \ v^* = 0 , \ T^* = T_H = 1 \tag{3.27.a}$$

For x=L:

$$x^* = 1, \ u^* = 0, \ v^* = 0, \ T^* = T_C = 0 \tag{3.27.b}$$

For y=H:

$$y^* = 1, \ u^* = 0, \ v^* = 0, \ \frac{\partial T^*}{\partial y^*} = 0 \tag{3.27.c}$$

For y=0:

$$y^* = 0, \ u^* = 0, \ v^* = 0, \ \frac{\partial T^*}{\partial y^*} = 0 \tag{3.27.d}$$

As seen from the above equations, the vertical walls have constant temperature and the horizontal upper and lower walls are adiabatic and derivative of the temperature of these boundaries are set to be zero. The no-slip and impermeability conditions are satisfied by equating the horizontal and vertical components of velocity to zero. The boundary conditions of streamfunction and vorticity will be presented later.

3.5 Overview of Numerical Methods to be Used

Presently, the finite difference method (FDM) and the finite element method (FEM) are widely used for the solution of partial differential equations of heat, mass and momentum transfer. Extensive amount of literature exist on the application of these methods for the solution of such problems.

Each method has its advantages depending on the nature of the physical problem to be solved; but there is no best method for all problems.

The accuracy of the FDM can readily be examined by the order of the truncation error in the Taylor's series expansion; but, in the case of FEM no Taylor's series expansion is involved in the formulation to make such assessments. The dimension of the problem is another factor that deserves some consideration. For example, an efficient method for one dimensional problems may not be so efficient for two or three dimensional problems.

Finite difference methods are simple to formulate and can readily be extended to two or three dimensional problems and require less computational work than the FEMs. Furthermore, FDM is very easy to learn and apply for the solution of partial differential equations encountered in the modeling of engineering problems for simple geometries (i.e., not very irregular).

In FDM, the solution domain is divided into a grid of discrete points or nodes. The partial differential equation is then written for each node and its derivatives replaced by finite divided differences.

In finite-element method (FEM) the underlying principle is its ability to easily solve problems described by complex boundary shapes. The FEM was initially developed to calculate stress in irregularly shaped objects and analyze structural problems in aircraft. Since its inception, the FEM has been found to be equally effective in nonstructural problems, particularly those in heat transfer and fluid dynamics. A detailed comparison of FDM and FEM was examined by D.W. Pepper and A.J. Baker, [22].

For the case being examined in this study (regular rectangular simple geometry), it is acceptable to use a finite difference method to solve the equations for computation. Followings are some of the FDM that may be used for the case:

3.5.1 Gauss-Seidel Iteration

The vorticity-stream function equation is in the form of Poisson's equation. The problem involves unknown internal node stream functions and finite difference equations provide algebraic equations for the determination of these unknown parameters. To solve this system of equations by the Gauss-Seidel iteration the second-order accurate standard finite-differencing scheme is solved for the main diagonal element $\psi_{i,j}$ and arranged in the form:

$$\psi_{i,j}^{p+1} = \frac{\psi_{i+1,j}^{p} + \psi_{i-1,j}^{p+1} + \beta^2\left(\psi_{i,j+1}^{p} + \psi_{i,j-1}^{p+1}\right) + (\Delta x)^2 \omega_{i,j}}{2(1+\beta^2)} \qquad (3.28)$$

where $\beta = \Delta x / \Delta y$, superscript p denotes the level of iteration, and the subscripts i and j denote column and row, respectively. After an initial guess is made for the unknown internal nodes, the iteration is considered to proceed by rows starting with the row next to the lower boundary and increasing j after each iteration. Therefore, the values of $\psi_{i-1,j}^{p+1}$ and $\psi_{i,j-1}^{p+1}$ at the iteration level p+1 appearing on the right-hand side of Equation 3.28 are actually known values, since the most recent values of ψ are used on the right-hand side of the equation.

3.5.2 Successive Over Relaxation (SOR)

The convergence rate is improved if successive over relaxation (SOR) is used. The application of the relaxation formula to the Gauss-Seidel iteration formula (Equation 3.28) gives

$$\psi_{i,j}^{p+1} = (1-\kappa)\psi_{i,j}^{p} + \frac{\kappa}{2(1+\beta^2)}\left[\psi_{i+1,j}^{p} + \psi_{i-1,j}^{p+1} + \beta^2(\psi_{i,j+1}^{p} + \psi_{i,j-1}^{p+1}) + (\Delta x)^2\omega_{i,j}\right] \quad (3.29)$$

where $\kappa=1$ corresponds to original Gauss-Seidel iteration, $0<\kappa<1$ to under-relaxation and $1<\kappa<2$ to successive over-relaxation (SOR).

The reduction in the computer time by the use of SOR depends on the proper choice of the value of the parameter κ. There is no general rule for the optimum value κ_{opt}. However, for the solution of Laplace's equation in a rectangular domain subject to boundary condition of the first kind at all boundaries, based on the work of Frankel and Young [23,24], the following optimum value κ_{opt} is suggested by Roache [25].

$$\kappa_{opt} = 2\left(\frac{1-\sqrt{1-\xi^2}}{\xi^2}\right) \quad (3.30)$$

where

$$\xi = \frac{1}{1+\beta^2}\left[Cos(\frac{\pi}{m-1}) + \beta^2 Cos(\frac{\pi}{n-1})\right] \quad (3.31)$$

$$\beta = \frac{\Delta x}{\Delta y} = \text{Grid aspect ratio} \quad (3.32)$$

m and n are the number of constant Δx and Δy subdivisions of the rectangular domain in the x- and y-directions, respectively.

24

The above results are for a rectangular region subject to boundary conditions of the first kind at all boundaries. For other geometries and boundary conditions, κ_{opt} can be estimated by examining the rate of convergence of the solution for several different values of κ over the region $1<\kappa<2$.

The stream function values at each node of the finite difference mesh covering the control volume are successively calculated from the finite difference form of the Poisson equation. The results are used to calculate the new values of the stream function each node, using the finite difference form of the momentum and energy equation. This iterations will continue until the desired accuracy is achieved.

The main handicap of this method is that it only facilitates the convergence of the Poisson equation, for some nonlinear equations of natural convection, the optimum value of κ does not accelerate the convergence of the momentum and energy equations simultaneously.

CHAPTER 4

FINITE DIFFERENCE FORMULATIONS
AND SOLUTIONS

The first step for solving a system of partial differential equations is to convert them to algebraic difference equations and simplified to a form that is suitable for computer programming. Secondly, the mesh size shall be chosen to get accurate results. The important point in choosing the structure is to get Nusselt number values that are close to experimental results. This can be reached by choosing fine grid structures. The disadvantage is that, the convergence is harder to achieve.

The method that will be presented here is as follows. The stream function values obtained from the solution of the nondimensional finite difference form of the stream function-vorticity equation are used to calculate the vorticity values from the momentum equation. Then the energy equation is solved in order to obtain the improved values of the temperature. These improved values are used in energy equation to obtain the new values of the stream function. Finally new values of stream function are used to get the improved values of vorticity. This continues until the convergence criterion is reached. Finite difference equations to be used in the FORTRAN code will be presented in the later sections.

4.1 Finite Difference Formulations

In this study the central difference approximation is used for the equations that will be used in computer programming. The advantage is that the error emerged by the central difference approximations (2nd order accurate) is less than that of forward and backward difference approximations. The approximation is as follows:

$$\left.\frac{\partial \eta}{\partial x}\right|_{i,j} = \frac{\eta_{i+1,j} - \eta_{i-1,j}}{2\Delta x} \qquad (4.1.a)$$

$$\left.\frac{\partial \eta}{\partial y}\right|_{i,j} = \frac{\eta_{i,j+1} - \eta_{i,j-1}}{2\Delta y} \qquad (4.1.b)$$

$$\left.\frac{\partial^2 \eta}{\partial x^2}\right|_{i,j} = \frac{\eta_{i+1,j} + \eta_{i-1,j} - 2\eta_{i,j}}{(\Delta x)^2} \qquad (4.1.c)$$

$$\left.\frac{\partial^2 \eta}{\partial y^2}\right|_{i,j} = \frac{\eta_{i,j+1} + \eta_{i,j-1} - 2\eta_{i,j}}{(\Delta y)^2} \qquad (4.1.d)$$

$$\left.\frac{\partial^2 \eta}{\partial x \partial y}\right|_{i,j} = \frac{\eta_{i+1,j+1} - \eta_{i+1,j-1} - \eta_{i-1,j+1} + \eta_{i-1,j-1}}{\Delta x \Delta y} \qquad (4.1.e)$$

where, η is any variable (ω, ψ, T) whose derivatives will be calculated as finite difference form.

4.2 Boundary Conditions

The finite difference form of the boundary conditions that will be used in the model are presented below: (There are n x m nodes in the medium.)

1. For the boundary nodes at the bottom of the medium with impermeable, no-slip boundary condition (i.e. the fluid velocity matches the velocity of the solid boundary) and insulated boundary condition:

$$\psi_{i,j} = 0$$

$$\omega_{i,j} = -2 \frac{\psi_{i,j+1}}{(\Delta y)^2}$$ (4.2.a)

$$T_{i,j} = T_{i,j+1}$$

For j=1 and 2≤i≤n-1

2. For the boundary nodes at the top of the medium with impermeable, no-slip boundary and insulated wall boundary condition:

$$\psi_{i,j} = 0$$

$$\omega_{i,j} = -2 \frac{\psi_{i,j-1}}{(\Delta y)^2}$$ (4.2.b)

$$T_{i,j} = T_{i,j-1}$$

For j=m and 2≤i≤n-1

3. For the boundary nodes at the left side of the medium with impermeable, no-slip boundary and constant temperature wall boundary condition

$$\psi_{i,j} = 0$$

$$\omega_{i,j} = -2 \frac{\psi_{i+1,j}}{(\Delta x)^2}$$ (4.2.c)

$$T_{i,j} = 1$$

For i=1 and 2≤j≤m-1

4. For the boundary nodes at the right side of the medium with impermeable, no-slip boundary and constant temperature wall boundary condition:

$$\psi_{i,j} = 0$$

$$\omega_{i,j} = -2 \frac{\psi_{i-1,j}}{(\Delta x)^2}$$ (4.2.d)

$$T_{i,j} = 0$$

For i=n and 2≤j≤m-1

For the corner boundary nodes the average of the two neighboring nodes are used.

4.3 Formulation of the Finite Difference Equations for Computer Programming

4.3.1 Finite Difference Form of the Vorticity-Stream Function Equation

The nondimensionalized vorticity-stream function equation is as in the Chapter 3:

$$\omega^* = -\frac{1}{A}\frac{\partial^2 \psi^*}{\partial x^{*2}} - A\frac{\partial^2 \psi^*}{\partial y^{*2}} \qquad (3.25)$$

Using the central difference approximations for the derivatives the finite difference form of the vorticity-stream function is:

$$\omega_{i,j}^* = -\frac{1}{A}\left[\frac{\psi_{i+1,j}^* + \psi_{i-1,j}^* - 2\psi_{i,j}^*}{(\Delta x)^2}\right] - A\left[\frac{\psi_{i,j+1}^* + \psi_{i,j-1}^* - 2\psi_{i,j}^*}{(\Delta y)^2}\right] \qquad (4.3)$$

where,

$$\Delta x = \frac{L}{n-1} \qquad (4.4.a)$$

$$\Delta y = \frac{H}{m-1} \qquad (4.4.b)$$

Δx is the distance between nodes in x-direction and Δy is the distance between nodes in y-direction, n and m are, as stated before, the number of nodes in x-direction and number of nodes in y-direction respectively. Finally, by simplifying the vorticity-stream function equation the resulting equation is as follows:

$$\psi_{i,j} = C_1\omega_{i,j} + C_2(\psi_{i+1,j} + \psi_{i-1,j}) + C_3(\psi_{i,j+1} + \psi_{i,j-1}) \qquad (4.5)$$

where the constants are:

$$C_1 = \frac{A(\Delta x)^2(\Delta y)^2}{2A^2(\Delta x)^2 + 2(\Delta y)^2} \qquad (4.6.a)$$

$$C_2 = \frac{(\Delta y)^2}{2A^2(\Delta x)^2 + 2(\Delta y)^2} \qquad (4.6.b)$$

$$C_3 = \frac{A^2 (\Delta x)^2}{2A^2 (\Delta x)^2 + 2(\Delta y)^2} \tag{4.6.c}$$

4.3.2 Finite Difference Form of the Energy Equation

The nondimensionalized form of the energy equation from Chapter 3 is;

$$Pr_m \left[\frac{\partial \psi^*}{\partial y^*} \frac{\partial T^*}{\partial x^*} - \frac{\partial \psi^*}{\partial x^*} \frac{\partial T^*}{\partial y^*} \right] = \frac{1}{A} \frac{\partial^2 T^*}{\partial x^{*2}} + A \frac{\partial^2 T^*}{\partial y^{*2}} \tag{3.26}$$

By applying the central difference to the partial derivatives the finite difference form of the energy equation is obtained as:

$$Pr_m \left[\left(\frac{\psi_{i,j+1} - \psi_{i,j-1}}{2\Delta y} \cdot \frac{T_{i+1,j} - T_{i-1,j}}{2\Delta x} \right) - \left(\frac{\psi_{i+1,j} - \psi_{i-1,j}}{2\Delta x} \cdot \frac{T_{i,j+1} - T_{i,j-1}}{2\Delta y} \right) \right] =$$

$$\frac{1}{A} \cdot \left(\frac{T_{i+1,j} + T_{i-1,j} - 2T_{i,j}}{(\Delta x)^2} \right) + A \cdot \left(\frac{T_{i,j+1} + T_{i,j-1} - 2T_{i,j}}{(\Delta y)^2} \right) \tag{4.7}$$

By simplifying the energy equation the resultant equation is as follows:

$$T_{i,j} = K_4 \cdot T_{i+1,j} + K_5 \cdot T_{i-1,j} + K_6 \cdot T_{i,j+1} + K_7 \cdot T_{i,j-1} \tag{4.8}$$

where the constants are:

$$K_4 = \frac{4\Delta y^2 - Pr_m \left(\psi_{i,j+1} - \psi_{i,j-1} \right) A \Delta x \Delta y}{\underbrace{4 \left(2\Delta y^2 + 2A^2 \Delta x^2 \right)}_{K_3}} \tag{4.9.a}$$

$$K_5 = \frac{4\Delta y^2 + Pr_m \left(\psi_{i,j+1} - \psi_{i,j-1} \right) A \Delta x \Delta y}{\underbrace{4 \left(2\Delta y^2 + 2A^2 \Delta x^2 \right)}_{K_3}} \tag{4.9.b}$$

$$K_6 = \frac{4A^2 \Delta x^2 + Pr_m \left(\psi_{i+1,j} - \psi_{i-1,j} \right) A \Delta x \Delta y}{\underbrace{4 \left(2\Delta y^2 + 2A^2 \Delta x^2 \right)}_{K_3}} \tag{4.9.c}$$

$$K_7 = \frac{4A^2 \Delta x^2 - Pr_m \left(\psi_{i+1,j} - \psi_{i-1,j} \right) A \Delta x \Delta y}{\underbrace{4 \left(2\Delta y^2 + 2A^2 \Delta x^2 \right)}_{K_3}} \tag{4.9.d}$$

4.3.3 Finite Difference Form of the Momentum Equation

The nondimensional form of the momentum equation is as follows:

$$C_{1n}^* \cdot F_1^*(\omega^*, \psi^*) = C_{2n}^* \cdot F_2^*(\omega^*) + C_{3n}^* \cdot F_3^*(\omega^*) + C_{4n}^* \cdot F_4^*(\psi^*) + C_{5n}^* \cdot F_5^*(T^*) \quad (3.19)$$

and by applying finite difference form and leaving $\omega_{i,j}$ alone, the equation becomes:

$$C_{1f} \cdot \omega_{i,j} = C_{2f} \cdot \omega_{i+1,j} - C_{2f} \cdot \omega_{i-1,j} - C_{3f} \cdot \omega_{i,j+1}$$

$$+ C_{3f} \cdot \omega_{i,j-1} - C_{4f} \cdot F_4(\psi^*) - C_{5f} \cdot F_5(T^*) \quad (4.10)$$

and the final form of momentum equation is:

$$\omega_{i,j} = \left(\frac{C_{2f}}{C_{1f}}\right) \cdot \left(\omega_{i+1,j} - \omega_{i-1,j}\right) + \left(\frac{C_{3f}}{C_{1f}}\right) \cdot \left(\omega_{i,j-1} - \omega_{i,j+1}\right) - \left(\frac{C_{4f}}{C_{1f}}\right) \cdot F_4(\psi^*)$$

$$- \left(\frac{C_{5f}}{C_{1f}}\right) \cdot F_5(T^*) \quad (4.11)$$

where the constants are as follows:

$$C_{1f} = C_{3n} - \frac{2C_{2n}}{\Delta x^2} - \frac{2K_{2n}A^2}{\Delta y^2} \quad (4.12.a)$$

$$C_{2f} = \left[\frac{1}{4\Delta x \Delta y} \cdot \left(\psi_{i,j+1} - \psi_{i,j-1}\right) - \frac{C_{2n}}{\Delta x^2}\right] \quad (4.12.b)$$

$$C_{3f} = -\left[\frac{1}{4\Delta x \Delta y} \cdot \left(\psi_{i+1,j} - \psi_{i-1,j}\right) + \frac{C_{2n}A^2}{\Delta y^2}\right] \quad (4.12.c)$$

$$C_{4f} = \frac{C_{4n}}{\Delta x^3} \quad (4.12.d)$$

$$C_{5f} = C_{5n} \quad (4.12.e)$$

and the functions $F_4(\psi^*)$ and $F_5(T^*)$ are as follows;

$$F_5(T^*) = \frac{T_{i+1,j}^* - T_{i-1,j}^*}{2\Delta x} \quad (4.12.f)$$

$$F_4(\psi^*) = \left(\frac{\psi_{i+1,j} + \psi_{i-1,j} - 2\psi_{i,j}}{(\Delta x)^2}\right) \cdot \sqrt{\left(\frac{\psi_{i+1,j} - \psi_{i-1,j}}{2\Delta x}\right)^2 + A^2 \cdot \left(\frac{\psi_{i,j+1} - \psi_{i,j-1}}{2\Delta y}\right)^2}$$

$$+ \left(\frac{\psi_{i+1,j} - \psi_{i-1,j}}{2\Delta x}\right) \cdot \frac{\left(\frac{\psi_{i+1,j} - \psi_{i-1,j}}{2\Delta x}\right) \cdot \left(\frac{\psi_{i+1,j} + \psi_{i-1,j} - 2\psi_{i,j}}{(\Delta x)^2}\right)}{\sqrt{\left(\frac{\psi_{i+1,j} - \psi_{i-1,j}}{2\Delta x}\right)^2 + A^2 \cdot \left(\frac{\psi_{i,j+1} - \psi_{i,j-1}}{2\Delta y}\right)^2}}$$

$$+ \left(\frac{\psi_{i+1,j} - \psi_{i-1,j}}{2\Delta x}\right) \cdot \frac{A^2 \cdot \left(\frac{\psi_{i,j+1} - \psi_{i,j-1}}{2\Delta y}\right) \cdot \left(\frac{\psi_{i+1,j+1} - \psi_{i+1,j-1} - \psi_{i-1,j+1} + \psi_{i-1,j-1}}{\Delta x \cdot \Delta y}\right)}{\sqrt{\left(\frac{\psi_{i+1,j} - \psi_{i-1,j}}{2\Delta x}\right)^2 + A^2 \cdot \left(\frac{\psi_{i,j+1} - \psi_{i,j-1}}{2\Delta y}\right)^2}}$$

$$+ A^2 \cdot \left(\frac{\psi_{i,j+1} + \psi_{i,j-1} - 2\psi_{i,j}}{(\Delta y)^2}\right) \cdot \sqrt{\left(\frac{\psi_{i+1,j} - \psi_{i-1,j}}{2\Delta x}\right)^2 + A^2 \cdot \left(\frac{\psi_{i,j+1} - \psi_{i,j-1}}{2\Delta y}\right)^2}$$

$$+ \left(\frac{\psi_{i,j+1} - \psi_{i,j-1}}{2\Delta y}\right) \cdot \frac{\left(\frac{\psi_{i+1,j} - \psi_{i-1,j}}{2\Delta x}\right) \cdot \left(\frac{\psi_{i+1,j+1} - \psi_{i+1,j-1} - \psi_{i-1,j+1} + \psi_{i-1,j-1}}{\Delta x \cdot \Delta y}\right)}{\sqrt{\left(\frac{\psi_{i+1,j} - \psi_{i-1,j}}{2\Delta x}\right)^2 + A^2 \cdot \left(\frac{\psi_{i,j+1} - \psi_{i,j-1}}{2\Delta y}\right)^2}}$$

$$+ \left(\frac{\psi_{i,j+1} - \psi_{i,j-1}}{2\Delta y}\right) \cdot \frac{A^2 \cdot \left(\frac{\psi_{i,j+1} - \psi_{i,j-1}}{2\Delta y}\right) \cdot \left(\frac{\psi_{i,j+1} + \psi_{i,j-1} - 2\psi_{i,j}}{(\Delta y)^2}\right)}{\sqrt{\left(\frac{\psi_{i+1,j} - \psi_{i-1,j}}{2\Delta x}\right)^2 + A^2 \cdot \left(\frac{\psi_{i,j+1} - \psi_{i,j-1}}{2\Delta y}\right)^2}} \tag{4.12.g}$$

4.4 Numerical Computing Strategy

For the rectangular control volume in our case, a grid structure should be formed in order to solve the problem easily with a computer program based solution technique. The values of the variables are calculated at the nodes which are the intersection points of the formed grid structure.

Initial values for the streamfunction and the vorticity are set to zero for the simplicity, the values for the temperature are taken as pure conduction situation in order to get a linear temperature variation inside the porous medium.
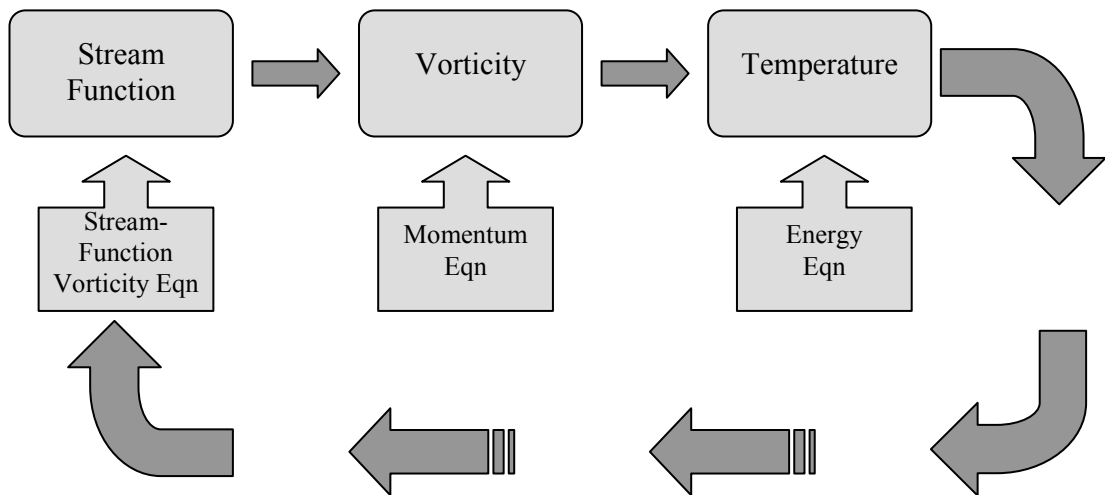

Figure 4.1: The flow-chart for the iteration procedure

The flow chart in Figure 4.1 shows the main iteration process of the program. For each internal node of the grid structure, values of streamfunction are calculated from the vorticity-streamfunction equation (Eqn. 4.5), using the previously calculated values of vorticity and streamfunction. Then the next step is to find new values of vorticity by using the final form of momentum equation (Eqn. 4.11). And as a final step for calculation process, the obtained values are substituted into the energy equation (Eqn. 4.8) to obtain the temperature for each node.

After applying the above mentioned procedures, now is the time for convergence criteria which is the final process for obtaining practical results. In order to reach the final converged values, we need to initiate the cycle for each node at first. Then as a secondary step the convergence criteria takes place which is the criteria to stop iteration process for streamfunction, vorticity and temperature values

of each node. When applying an iterative process, there is a need for a convergence criterion to check whether the process converges or not. If the convergence check fails, the secondary cycle is initiated repeating the same procedures (iterations) for each internal node. The chosen convergence criterion is as follows:

$$\left| \frac{\sum\limits_{i=1}^{i=m}\sum\limits_{j=1}^{j=n}\eta^{p+1} - \sum\limits_{i=1}^{i=m}\sum\limits_{j=1}^{j=n}\eta^{p}}{\sum\limits_{i=1}^{i=m}\sum\limits_{j=1}^{j=n}\eta^{p+1}} \right| < 0.00001 \qquad\qquad (4.13)$$

where, η is any variable (ω, ψ or T) used in the equations and p is the number of iterative cycles achieved.

For the selection of convergence criteria four different values of criterion are used to obtain the results and finally the criterion value of 0.00001 is chosen for the optimum process time and accuracy. The effects of convergence criterion to the program results will be presented in the later sections.

4.5 Computer Program

The computer program used in this study is a Compaq Visual FORTRAN 6.1 code which is a version of Fortran 90 free format source program. The objective of the code is mainly to determine the streamfunction, vorticity, temperature and Nusselt number for the defined rectangular control volume. The sequence and the main steps of the code are as follows;

The code does not contain any subroutine or sub functions. All functions are done in a main program. First of all, in the very early parts of the program, the general constants that are used in the entire program are set to their values such as, porosity of the medium, fluid Rayleigh number, Prandtl number, etc. Then the constants for the vorticity-streamfunction equation are set. After these steps the boundary and initial conditions are defined in accordance with the sections (4.2) and (4.4). Following the above mentioned steps, the main and the most important part of the program, the iteration cycle for evaluating the streamfunction, vorticity and temperature is compiled with the finite difference forms of equations as in section (4.3). Following the iteration procedure, in order to reach the converged values of the

variables, the termination process takes place with the convergence criteria of $1x10^{-5}$. The iteration procedure and the termination process for the iteration work together to get the final values. After reaching the convergence the final calculation process is for the Nusselt number. In order to get these values in to an Excel worksheet the program writes all the calculated values to a text file an also an Excel worksheet.

After completing the above mentioned issues on the computer programming code, then the outputs of the program are examined and the necessary graphs, tables and etc. are plotted with respect to the variables in the equations such as, Da (Darcy number), Ra_H (Rayleigh number based on height), Pr (Prandtl number), φ (porosity). In the later sections these graphs and the tables are presented.

CHAPTER 5

RESULTS AND DISCUSSION

In this chapter of the study, the results of the computer program will be presented. The outputs of the code are collected using the Microsoft Excel software and plotted versus thermodynamic properties of the medium and the fluid. Previously done research and studies are also included in the graphical demonstration of the results of FORTRAN code. As stated in Chapter 4 the computer program lets the user view the effects of the below mentioned variables on the Nusselt number.

Rayleigh number based on height: $\quad\quad\quad\quad\quad Ra_H = \dfrac{g\beta_f KH\Delta T}{\nu_f \alpha_f}$

Rayleigh number based on horizontal distance: $\quad Ra_L = \dfrac{g\beta_f KL\Delta T}{\nu_f \alpha_f}$

Fluid Rayleigh number: $\quad\quad\quad\quad\quad\quad\quad Ra_f = \dfrac{g\beta_f L^3\Delta T}{\nu_f \alpha_f}$

Darcy number: $\quad\quad\quad\quad\quad\quad\quad\quad\quad Da = \dfrac{K}{L^2}$

Fluid Prandtl number: $\quad\quad\quad\quad\quad\quad\quad Pr = \dfrac{\nu_f}{\alpha_f}$

Moreover the program was run for different values within the below stated ranges to have convection dominant situations.

$10 < Ra_L < 400$
$10^{-8} < Da < 10^{-1}$
$10^2 < Ra_f < 10^8$

5.1 Convergence Analysis of the Study

As stated in the previous sections the iterative solution method is used in order to achieve a converged value in the finite difference method solving system. In the iterative nature solution systems the convergence criteria is the most significant item. While keeping the convergence criteria to a minimum value you have to examine the process time and the relative change in final values. So the most applicable way is to find an optimum of these three parameters. In the following sections a detailed convergence analysis is presented to show the effect of these parameters on the results.

5.1.1 Convergence of the Temperature Values

In Figures 5.1 and 5.2 the behavior of the nondimensional temperature values are plotted against the convergence criteria defined in the Fortran code.

Table 5.1: Nondimensional temperature values of selected nodes for different convergence criteria.

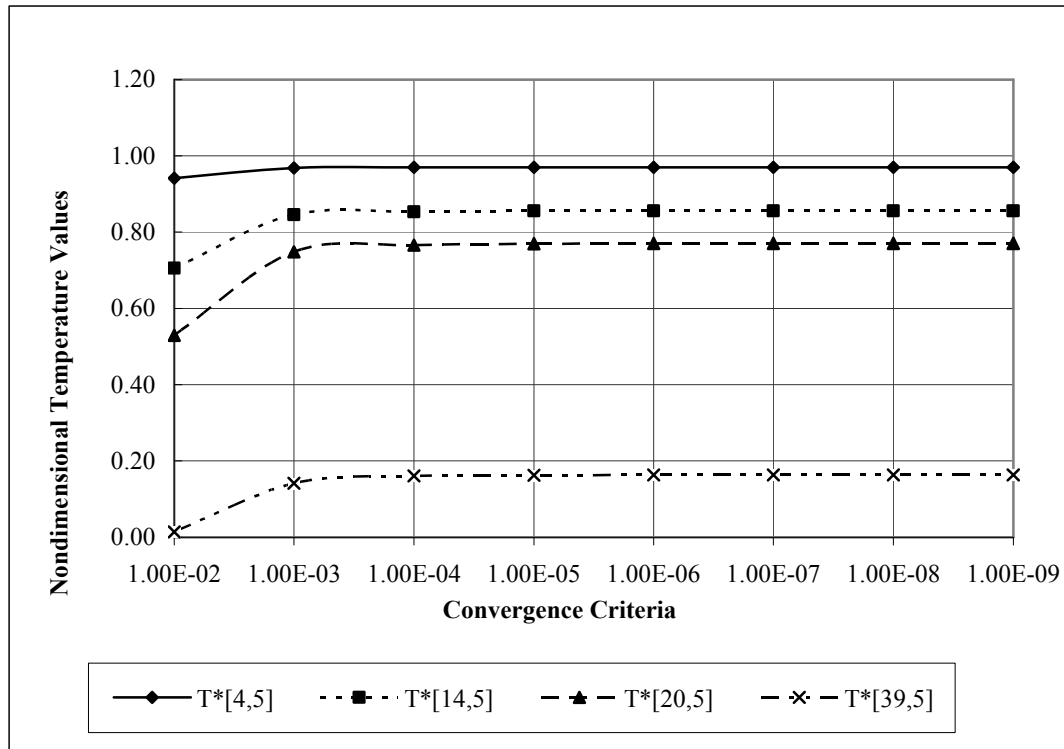| Convergence Criteria	Nondimensional Temperature Value (T*)			
	T*[4,5]	T*[14,5]	T*[20,5]	T*[39,5]
0.01	0.941176	0.705882	0.529412	0.014706
0.001	0.968357	0.845272	0.748485	0.141144
0.0001	0.969355	0.852997	0.766568	0.160887
0.00001	0.969911	0.855344	0.769821	0.162532
0.000001	0.969973	0.855629	0.770255	0.162783
0.0000001	0.969979	0.855652	0.770298	0.162808
0.00000001	0.969980	0.855661	0.770303	0.162810
0.000000001	0.969980	0.855661	0.770303	0.162811

Figure 5.1: Nondimensional temperature values of selected nodes versus convergence criteria

Table 5.2: % Difference of nondimensional temperature values from the final value for different convergence criteria

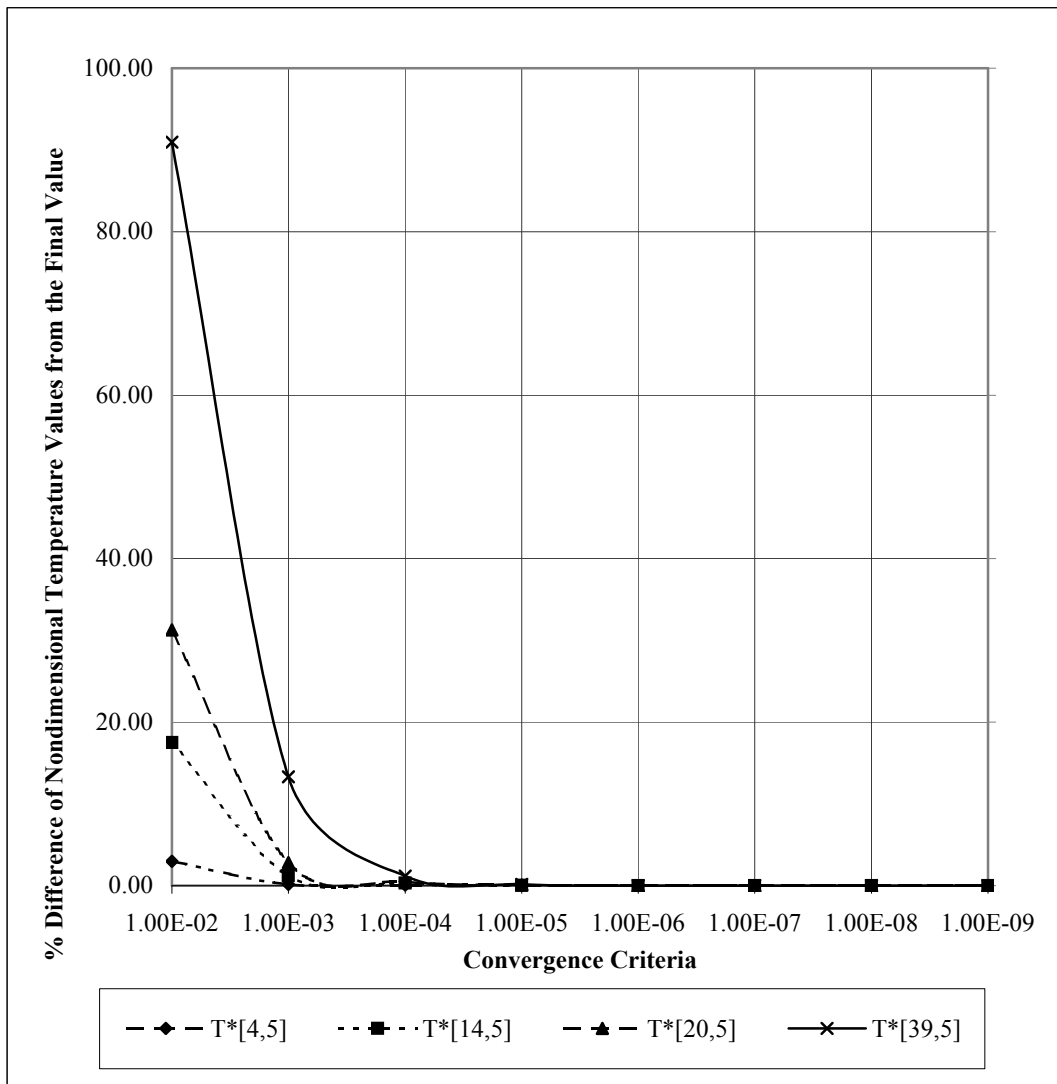| Convergence	% Difference in Nondimensional Temperature Value (T*)			
Criteria	T*[4,5]	T*[14,5]	T*[20,5]	T*[39,5]
0.01	2.969491	17.50446	31.272288	90.967538
0.001	0.167294	1.214223	2.832481	13.307923
0.0001	0.064417	0.311314	0.484912	1.181453
0.00001	0.007101	0.037087	0.062558	0.171156
0.000001	0.000714	0.003711	0.006239	0.016971
0.0000001	0.000070	0.000367	0.000615	0.001670
0.00000001	0.000006	0.000034	0.000056	0.000154
0.000000001	0.000000	0.000000	0.000000	0.000000

Figure 5.2: % Difference of nondimensional temperature values from the final value versus convergence criteria

5.1.2   Convergence of the Streamfunction Values

In the Figures 5.3 and 5.4 the behavior of the nondimensional streamfunction values are plotted against the convergence criteria defined in the Fortran code.

Table 5.3: Nondimensional streamfunction values of selected nodes for different convergence criteria.

Convergence Criteria	Nondimensional Streamfunction Value (ψ *)			
	ψ*[4,5]	ψ *[14,5]	ψ *[20,5]	ψ *[39,5]
0.001	0.426727	1.623231	1.997789	0.843549
0.0001	0.400440	1.494066	1.832465	0.890755
0.00001	0.394024	1.474766	1.816056	0.895587
0.000001	0.393492	1.473351	1.815032	0.896434
0.0000001	0.393438	1.473208	1.814929	0.896518
0.00000001	0.393433	1.473194	1.814919	0.896526
0.000000001	0.393432	1.473193	1.814918	0.896527
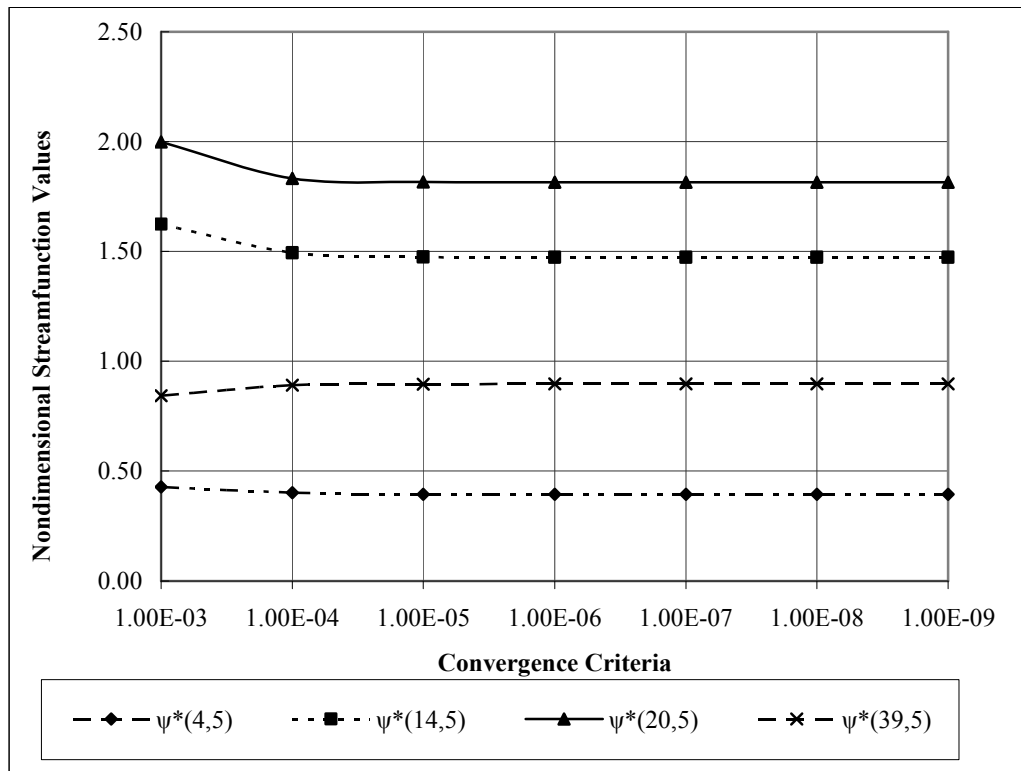
Figure 5.3: Nondimensional streamfunction values of selected nodes versus convergence criteria

Table 5.4: % Difference of nondimensional streamfunction values from the final value for different convergence criteria

Convergence Criteria	% Difference in Nondimensional Streamfunction Value (ψ *)			
	ψ*[4,5]	ψ *[14,5]	ψ *[20,5]	ψ *[39,5]
0.001	-8.46250	-10.184535	-10.076008	5.909242
0.0001	-1.781134	-1.416874	-0.966824	0.643830
0.00001	-0.150291	-0.106780	-0.062680	0.104773
0.000001	-0.015113	-0.010707	-0.006358	0.010391
0.0000001	-0.001489	-0.001055	-0.000616	0.001027
0.00000001	-0.000134	-0.000096	-0.000054	0.000094
0.000000001	0.000000	0.000000	0.000000	0.000000
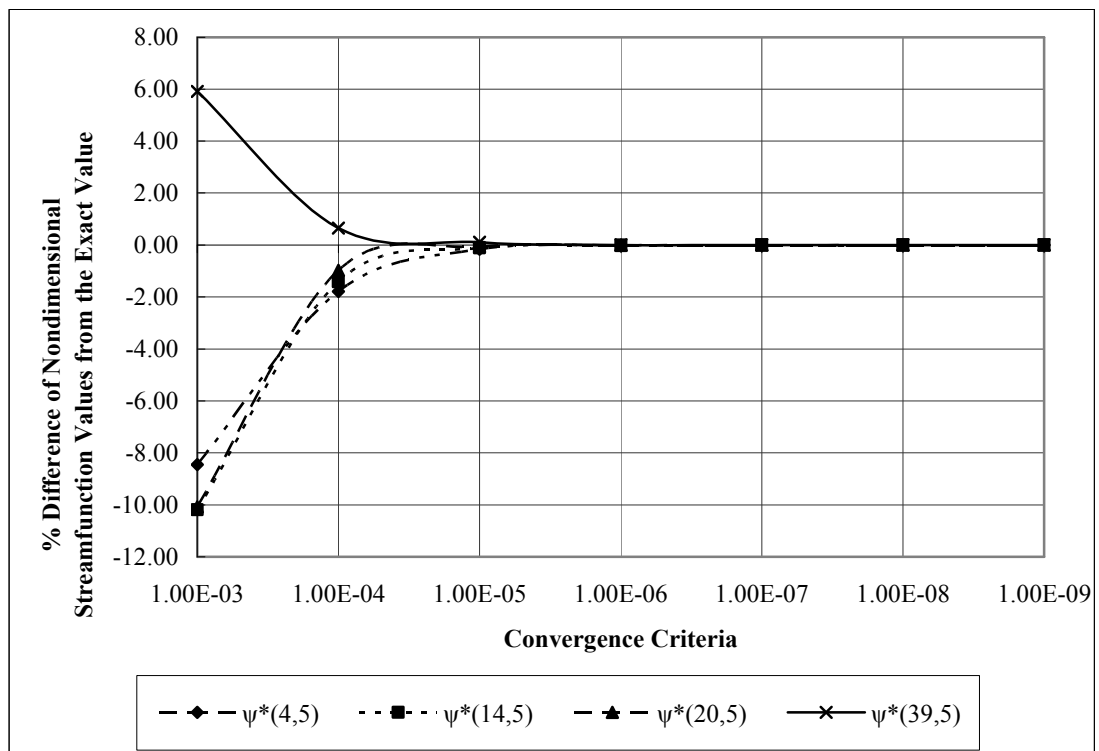
Figure 5.4: % Difference of nondimensional streamfunction values from the final value versus convergence criteria

5.1.3   Convergence of the Vorticity Values

In the Figures 5.5 and 5.6 the behavior of the nondimensional vorticity values are plotted against the convergence criteria defined in the Fortran code.

Table 5.5: Nondimensional vorticity values of selected nodes for different convergence criteria.

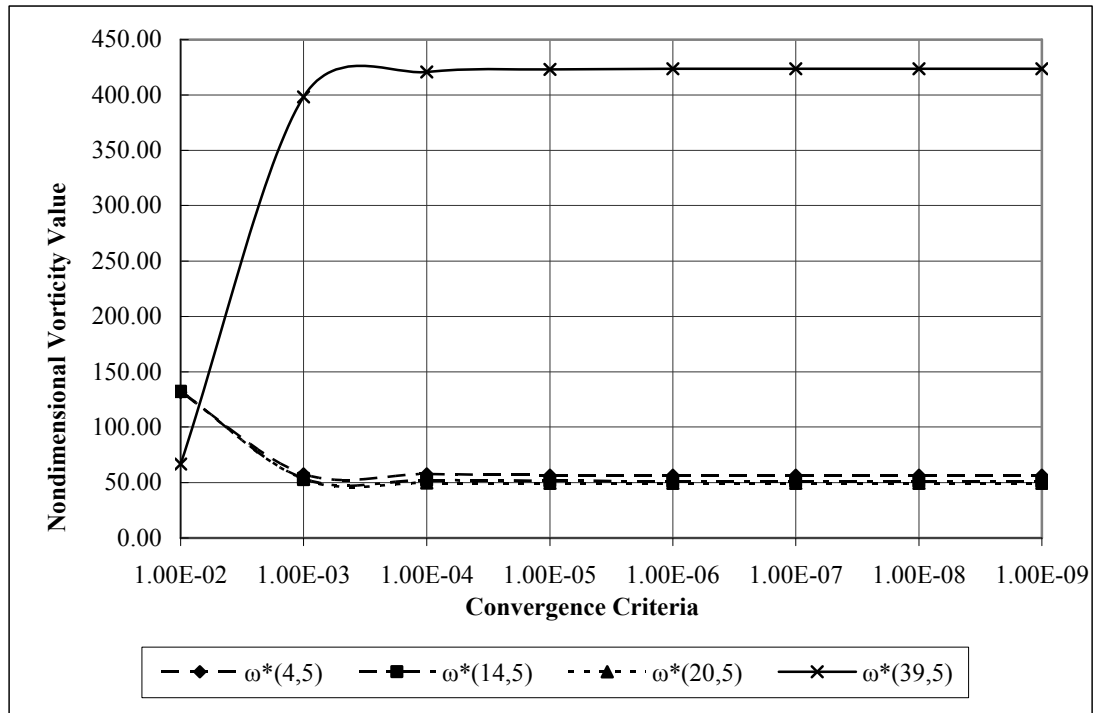| Convergence Criteria	Nondimensional Vorticity Value (ω*)			
	ω*[4,5]	ω *[14,5]	ω *[20,5]	ω *[39,5]
0.01	131.302461	132.336337	132.336337	66.685096
0.001	57.722439	53.643476	53.643476	398.2759970
0.0001	57.545847	52.027357	49.783828	420.803220
0.00001	56.453203	51.417849	49.467577	423.210225
0.000001	56.361820	51.347788	49.403048	423.607089
0.0000001	56.352662	51.340679	49.396459	423.647141
0.00000001	56.351737	51.340679	49.395797	423.651169

Figure 5.5: Nondimensional vorticity values of selected nodes versus convergence criteria

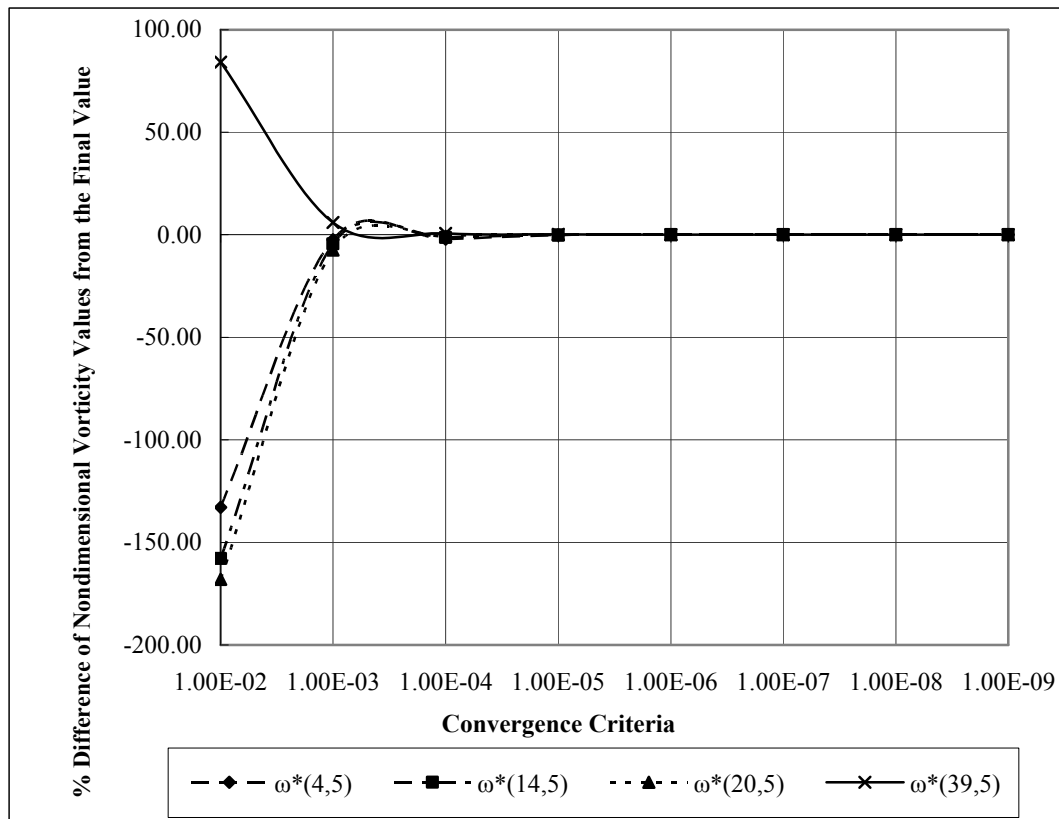**Table 5.6:** % Difference of nondimensional vorticity values from the final value for different convergence criteria

Convergence	% Difference in Nondimensional Vorticity Value (ω *)			
Criteria	ω*[4,5]	ω *[14,5]	ω *[20,5]	ω *[39,5]
0.01	-133.005549	-157.765124	-167.910474	84.259448
0.001	-2.433571	-4.486927	-7.439551	5.989733
0.0001	-2.119196	-1.339045	-0.785689	0.672333
0.00001	-0.180221	-0.151844	-0.145449	0.104176
0.000001	-0.018056	-0.015380	-0.014813	0.010499
0.0000001	-0.001804	-0.001532	-0.001474	0.001045
0.00000001	-0.000163	-0.000138	-0.000134	0.000094
0.000000001	0.000000	0.000000	0.000000	0.000000

43

Figure 5.6: % Difference of nondimensional vorticity values from the final value versus convergence criteria

5.1.4 Convergence Behavior for Different Number of Iterations

In this section of convergence analysis, the number of iterations required to get the converged value of temperature, streamfunction and vorticity values are examined to have an idea for the convergence time and rate.
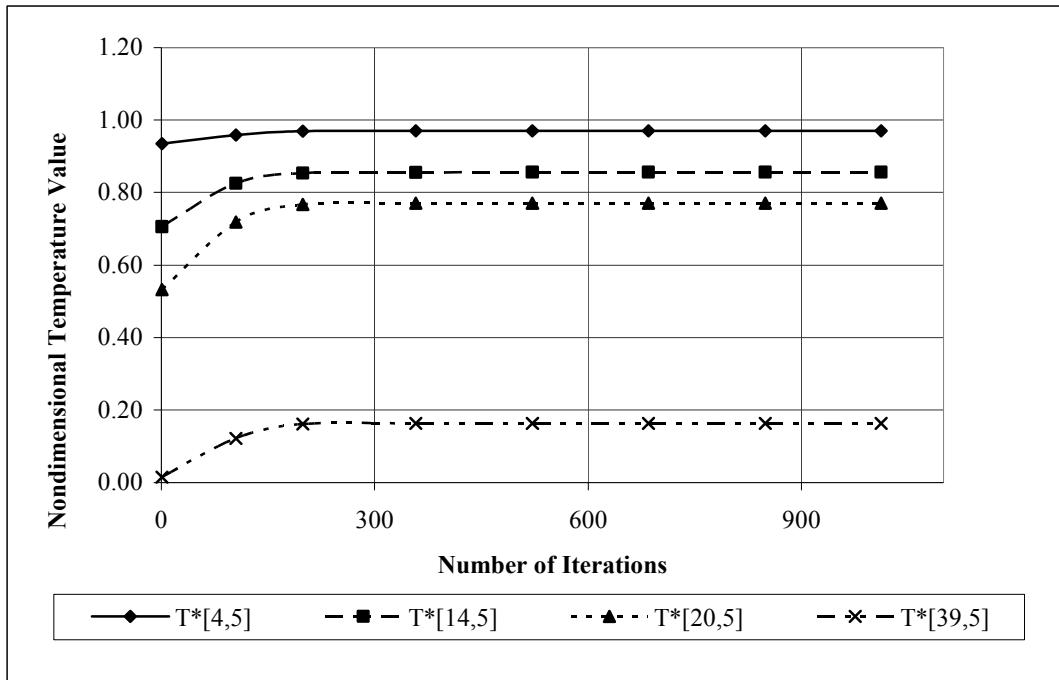
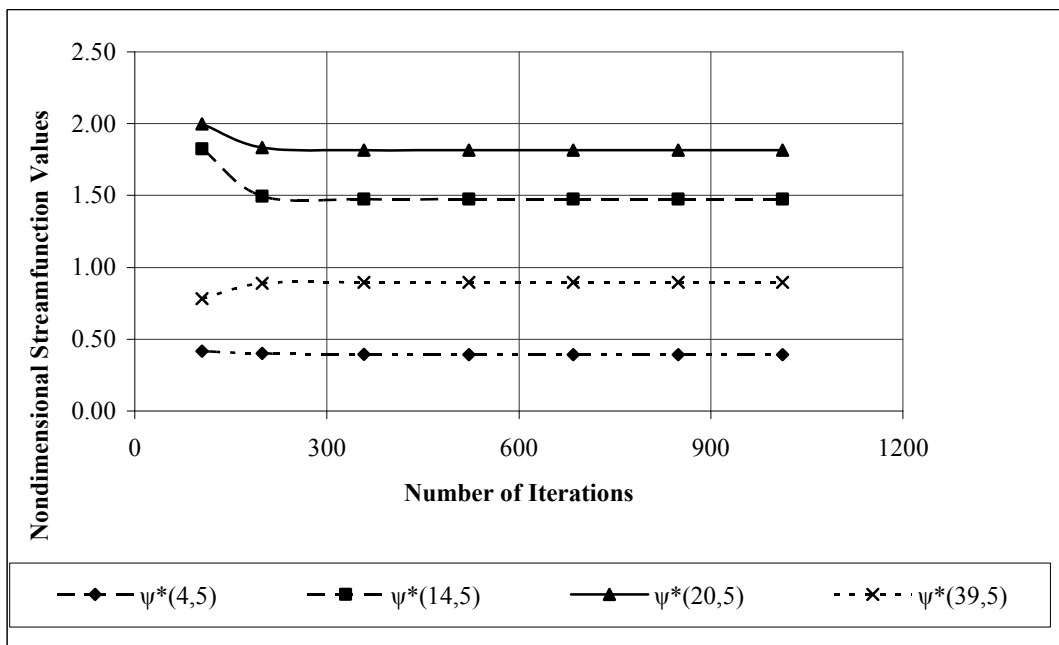**Figure 5.7:** Nondimensional temperature values for different number of iterations

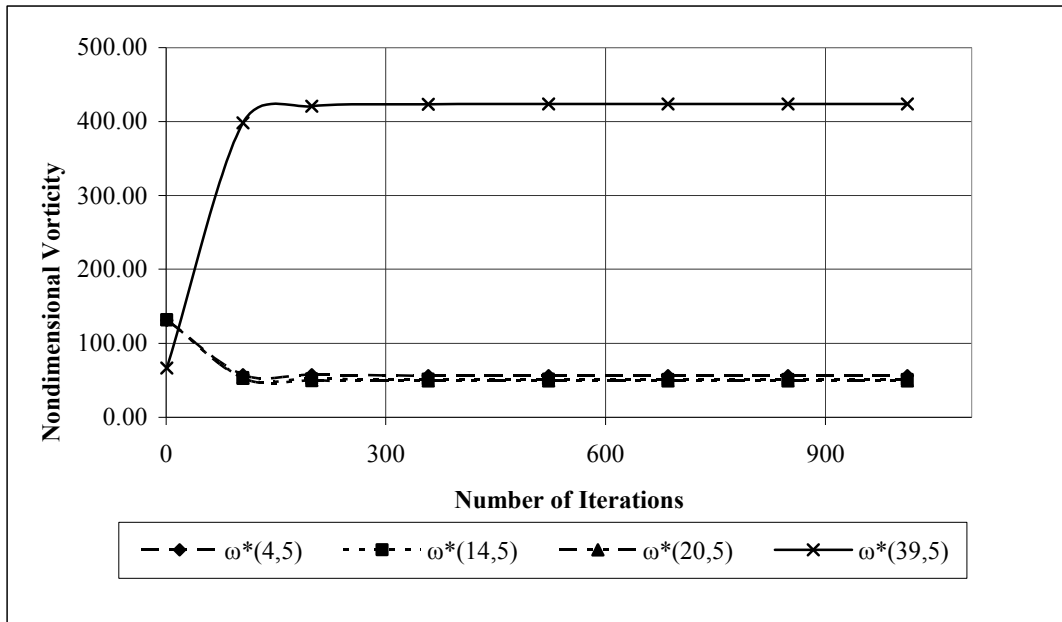**Figure 5.8:** Nondimensional streamfunction values for different number of iterations

45

Figure 5.9: Nondimensional vorticity values for different number of iterations

5.1.5   Convergence Behavior for Different Grid Structures

While deciding on the grid structure consisting of nodal points to be used in the finite difference equations a convergence analysis is made. The change in the final converged result has a significant importance as well as the computing time required. Figures 5.10 and 5.11 show the change in the Nusselt number and the temperature values for different grid structures, different node numbers.

Table 5.7: Comparison of Nusselt number values for different grid sizes (Da=0.00001, Ra_H=80, Pr=0.7, A=1, φ=0.5)

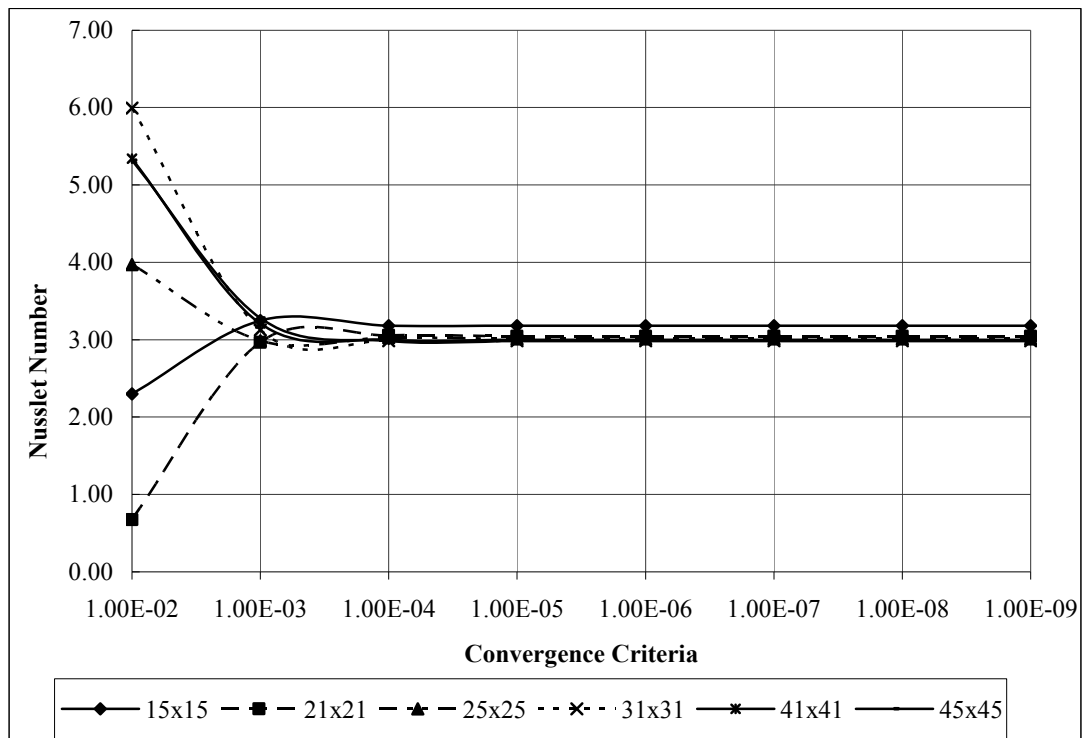| Convergence Criteria	Grid Structure					
	15x15	**21x21**	**25x25**	**31x31**	**41x41**	**45x45**
0.01	2.297941	0.676471	3.970588	5.992950	5.337036	5.319148
0.001	3.247451	2.967594	2.985676	3.126098	3.208922	3.280692
0.0001	3.181661	3.056494	3.028348	2.986219	2.997942	2.994086
0.00001	3.181397	3.044904	3.011398	2.988179	2.997748	2.992283
0.000001	3.181354	3.044919	3.011451	2.988256	2.997820	2.992341
0.0000001	3.181350	3.044926	3.011459	2.988260	2.997832	2.992354
0.00000001	3.181349	3.044927	3.011460	2.988266	2.997833	2.992355
0.000000001	3.181349	3.044927	3.011460	2.988266	2.997833	2.992355

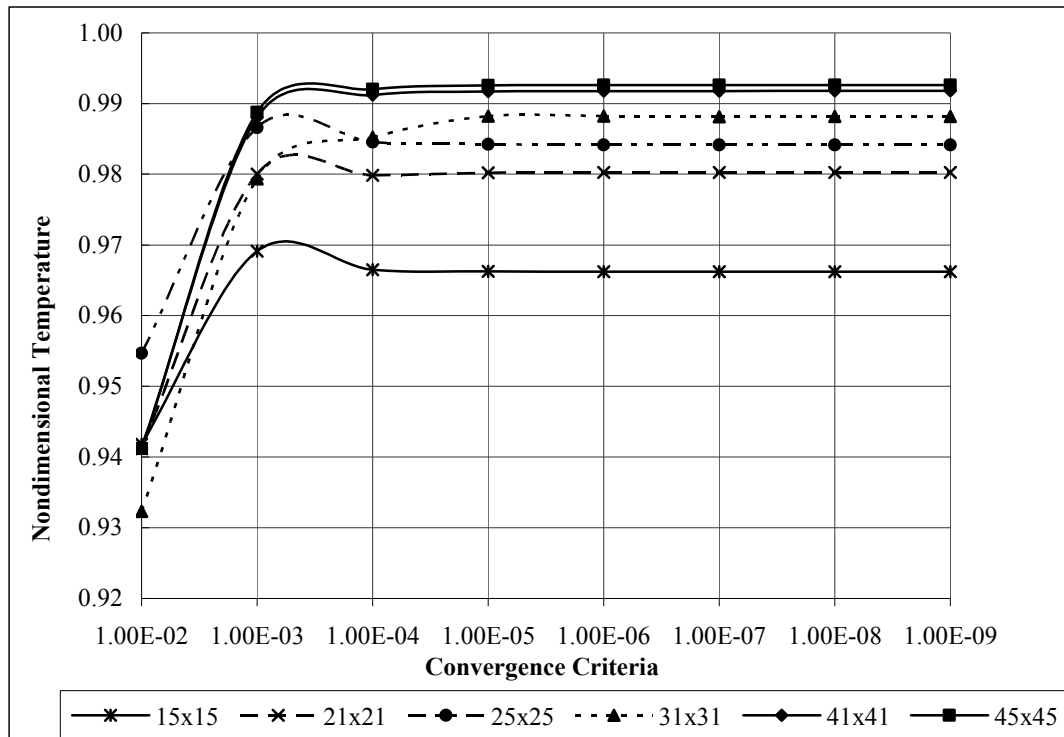**Figure 5.10:** Comparison of Nusselt number values for different grid sizes (Da=0.00001, Ra_H=80, Pr=0.7, A=1, φ=0.5)

Table 5.8: Comparison of Nondimensional temperature values T*(3,3) for different grid sizes (Da=0.00001, Ra_H=80, Pr=0.7, A=1, φ=0.5)

Convergence Criteria	Grid Structure					
	15x15	21x21	25x25	31x31	41x41	45x45
0.01	0.941783	0.941176	0.954656	0.932312	0.941373	0.941176
0.001	0.969111	0.980016	0.986575	0.979344	0.988016	0.988764
0.0001	0.966491	0.979837	0.984535	0.985232	0.991203	0.992022
0.00001	0.966262	0.980192	0.984234	0.988232	0.991711	0.992564
0.000001	0.966239	0.980221	0.984142	0.988232	0.991767	0.992625
0.0000001	0.966237	0.980224	0.984152	0.988123	0.991773	0.992631
0.00000001	0.966237	0.980225	0.984150	0.988167	0.991774	0.992630
0.000000001	0.966237	0.980225	0.984150	0.988166	0.991774	0.992630

Figure 5.11: Comparison of Nondimensional temperature values T*(3,3) for different grid sizes (Da=0.00001, Ra_H=80, Pr=0.7, A=1, φ=0.5)

Several grid sizes are used in order to find the optimum grid structure. As seen from Figure 5.10 and 5.11 after 41x41 grid size there occurs a negligible difference in the final converged values. Hence, 41x41 grid size is chosen for this case.

5.2   Error Analysis for the Finite Difference Method

Throughout the study first degree central difference approximations are used as the finite difference approximation except the calculations of Nusselt number values. For Nusselt number approximation three point approximation finite difference method is used for more accurate results. Due to this situation for temperature, stream function and vorticity values, some round off errors occur.

5.3   Temperature and Flow Fields within the Medium

In this section the obtained flow and temperature field graphs are presented for different cases as used in the previous sections in order to investigate the effects of some variables on Nusselt number. Furthermore, the obtained graphs and values are compared with previously done studies of some researchers. At first the temperature fields, in other words the isotherms will be presented.

5.3.1   Temperature Fields (Isotherms)

In order to observe the behavior of temperature distribution within the control volume, corresponding Figures 5.12 to 5.17 are examined in detail. The examinations are done in two ways: first Darcy number is kept constant and Rayleigh number based on height is changed; and after that Rayleigh number is kept constant and Darcy number is changed.

As it can be seen from the graphs, for constant Darcy number the hotter regions of the control volume are formed at the top side, whereas the colder ones at

the bottom. As a general effect of the buoyancy forces hotter regions begin to penetrate to the top portion of the control volume. When Figures 5.12, 5.13 and 5.14 (Da=0,001) and Figures 5.15, 5.16 and 5.17 (Da=0,000001) are examined, it is obvious that through an increase in Rayleigh number, hotter regions will begin to penetrate to the right hand side of the control volume. Another important issue to examine is when the Rayleigh number is kept constant and Darcy number is changing. For the same Rayleigh number regimes, through a decrease in Darcy number results in an increase in the amount of hotter regions in the upper half of the control volume. This situation can easily be examined as Figures 5.12 and 5.15, 5.13 and 5.16, 5.14 and 5.17 are observed together.
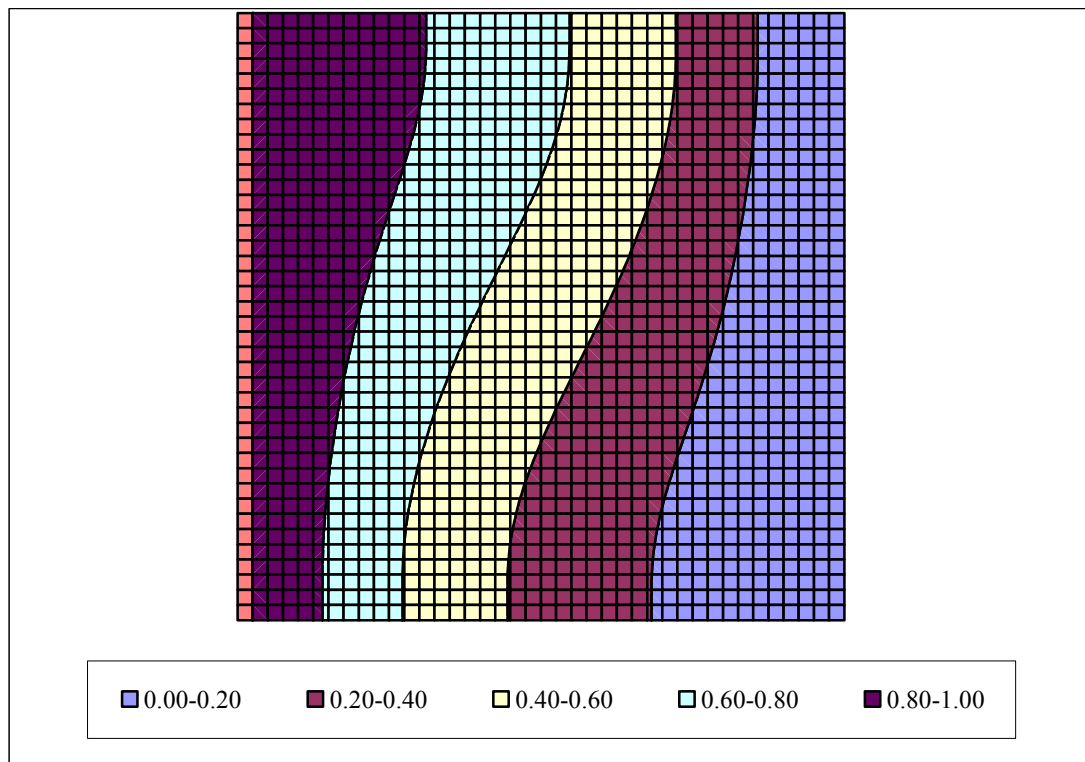
Figure 5.12: Temperature fields for Da=0.001, Ra_H=20, Pr=0.7, A=1, φ=0.5

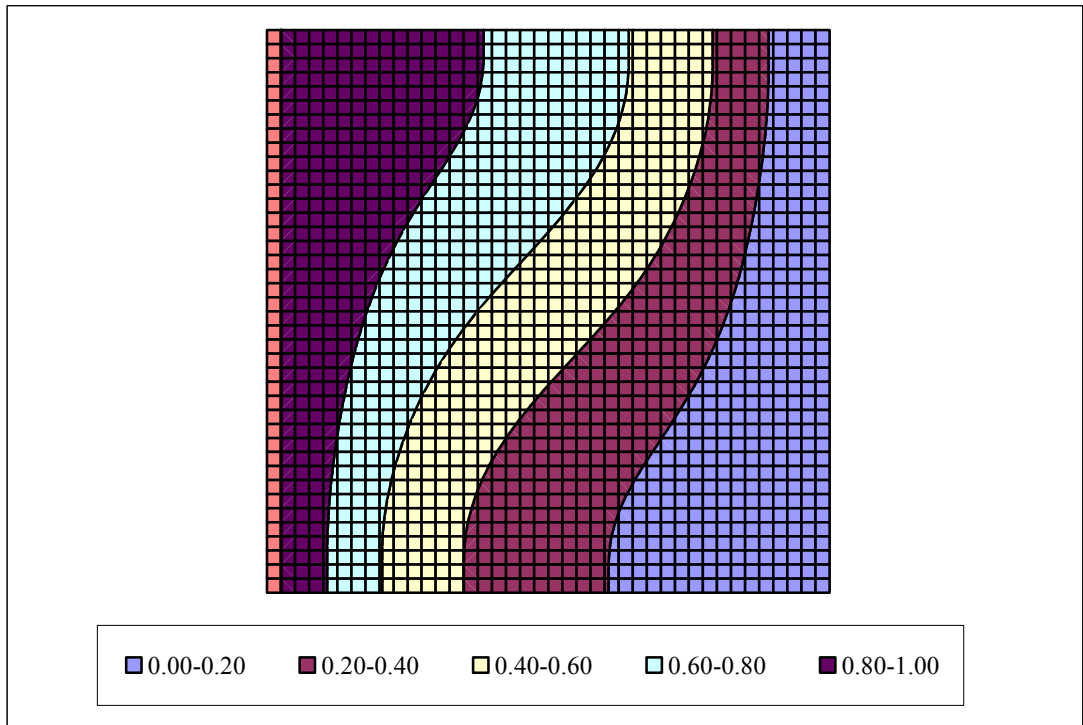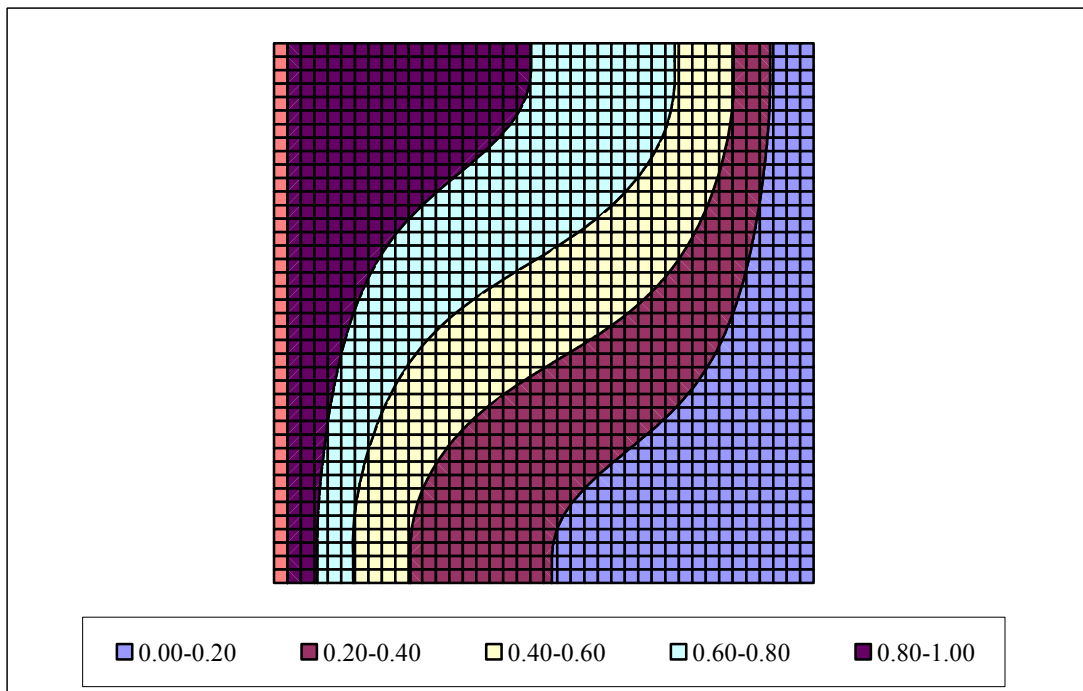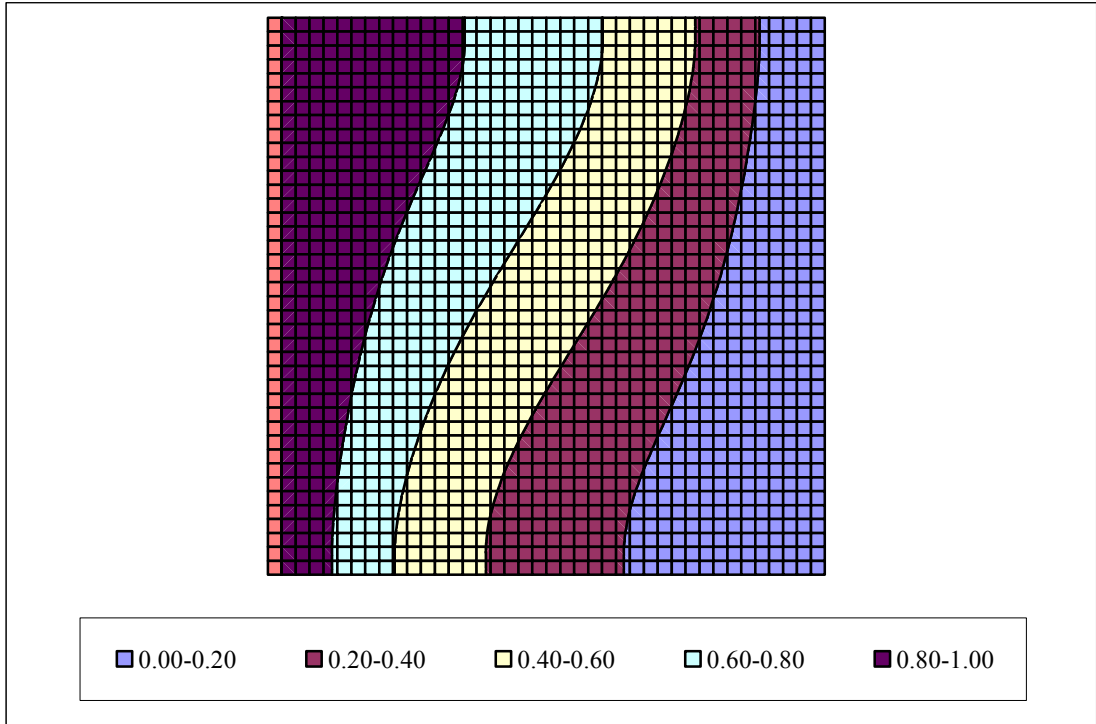**Figure 5.13:** Temperature fields for Da=0.001, Ra$_H$=40, Pr=0.7, A=1, φ=0.5

Figure 5.14: Temperature fields for Da=0.001, Ra$_H$=80, Pr=0.7, A=1, φ=0.5

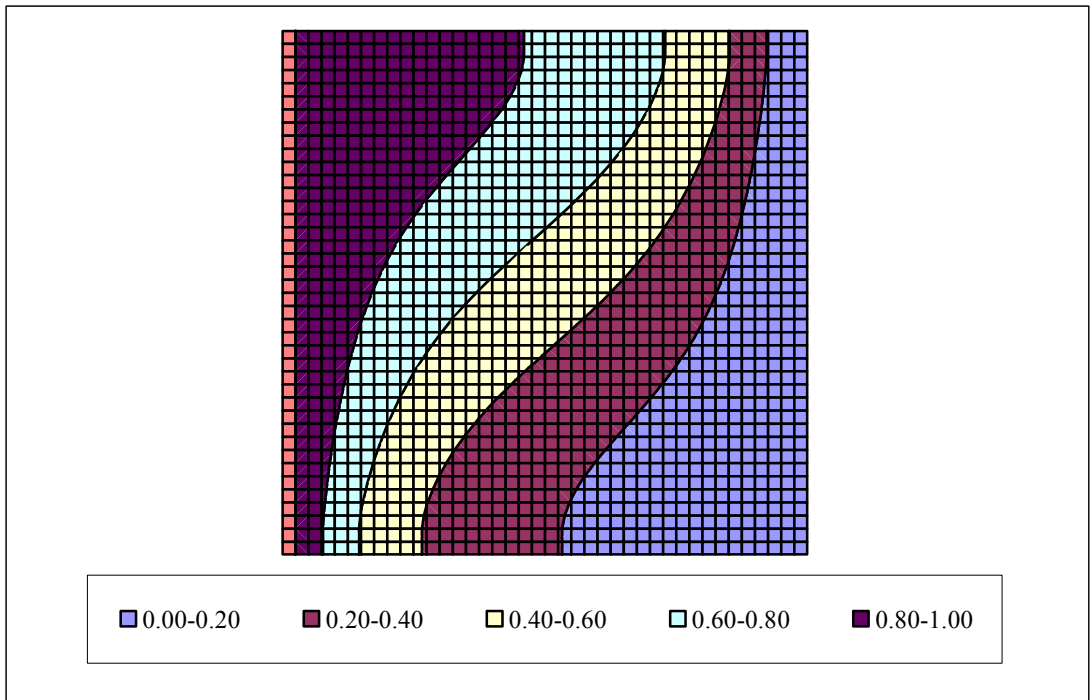**Figure 5.15:** Temperature fields for Da=0.000001, Ra$_H$=20, Pr=0.7, A=1, φ=0.5

Figure 5.16: Temperature fields for Da=0.000001, Ra$_H$=40, Pr=0.7, A=1, φ=0.5
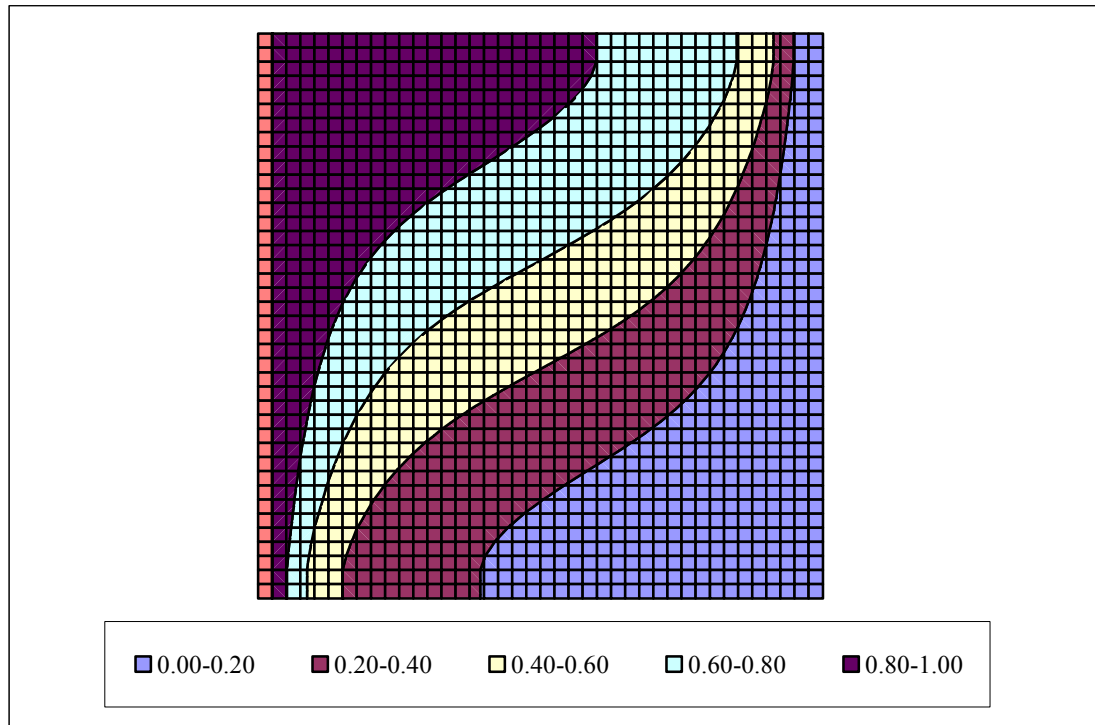
Figure 5.17: Temperature fields for Da=0.000001, Ra_H=80, Pr=0.7, A=1, φ=0.5

5.3.2 Flow Fields (Streamlines)

As mentioned in the previous section 5.3.1 the streamlines of the control volume are plotted for two cases with three sub cases; these are keeping Rayleigh number constant while decreasing Darcy number, and for the next case, keeping Darcy number constant while changing Rayleigh number.

When Figures 5.18 through 5.23 are examined, it may be concluded that for a constant Darcy number regime in a control volume the shape of the streamlines transform from circular to elliptical due to an increase in the Rayleigh number based on height. And also the elliptical shape rotates as Reyleigh number increases towards the right top side. This is due to the accumulation of the hot nodes at the right top side as Reyleigh number increases. This phenomenon is mainly due to the density gradients formed due to the temperature differences in the control volume, and it can be observed much easier in Figures 5.22 and 5.23. The opposite condition is also

valid for the below regions that causes the deviation in the streamlines. The code does not give applicable results for higher Rayleigh numbers that results a non-unicellular patterns.
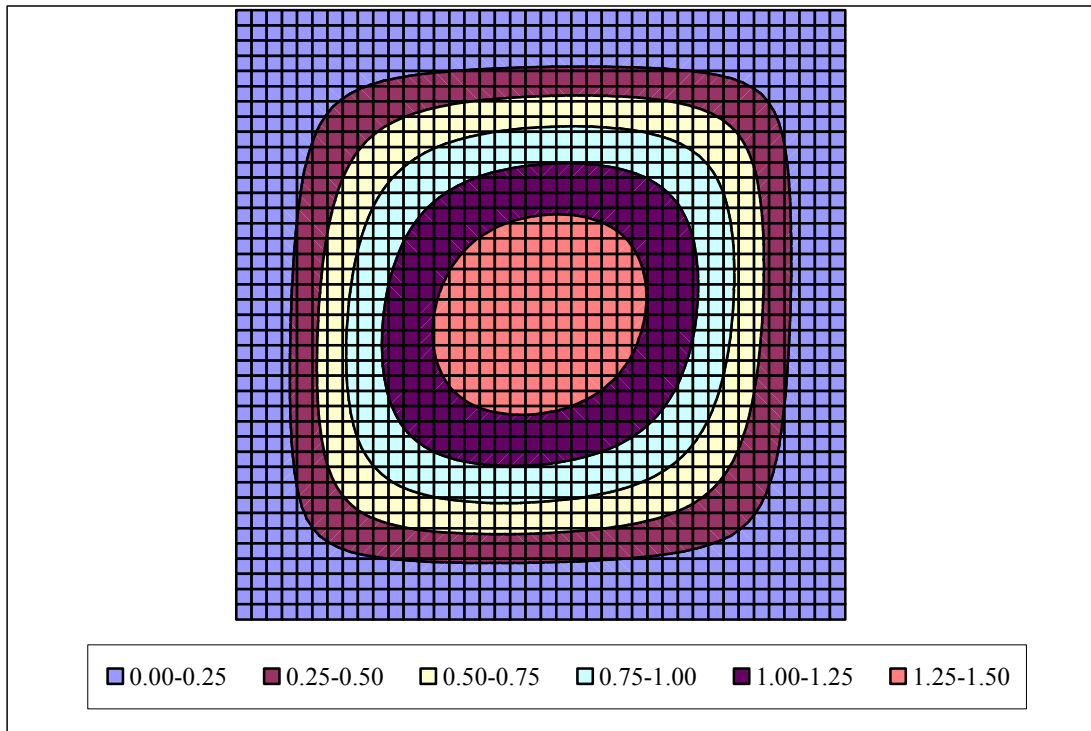

Figure 5.18: Streamlines for Da=0.001, Ra$_H$=20, Pr=0.7, A=1, φ=0.5
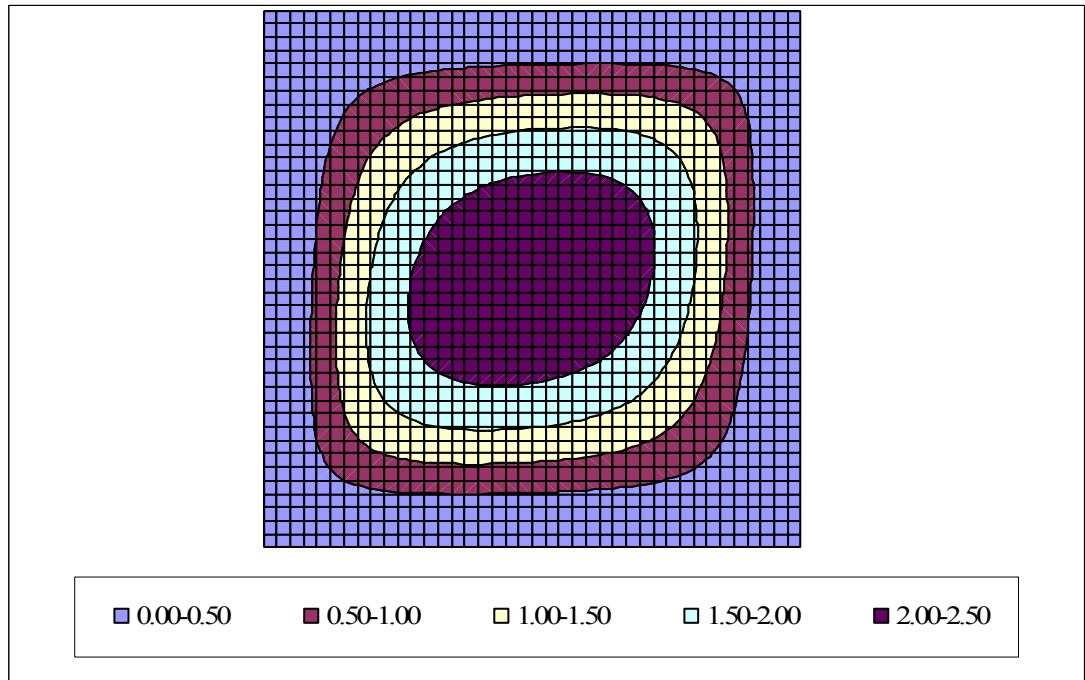
Figure 5.19: Streamlines for Da=0.001, Ra$_H$=40, Pr=0.7, A=1, φ=0.5

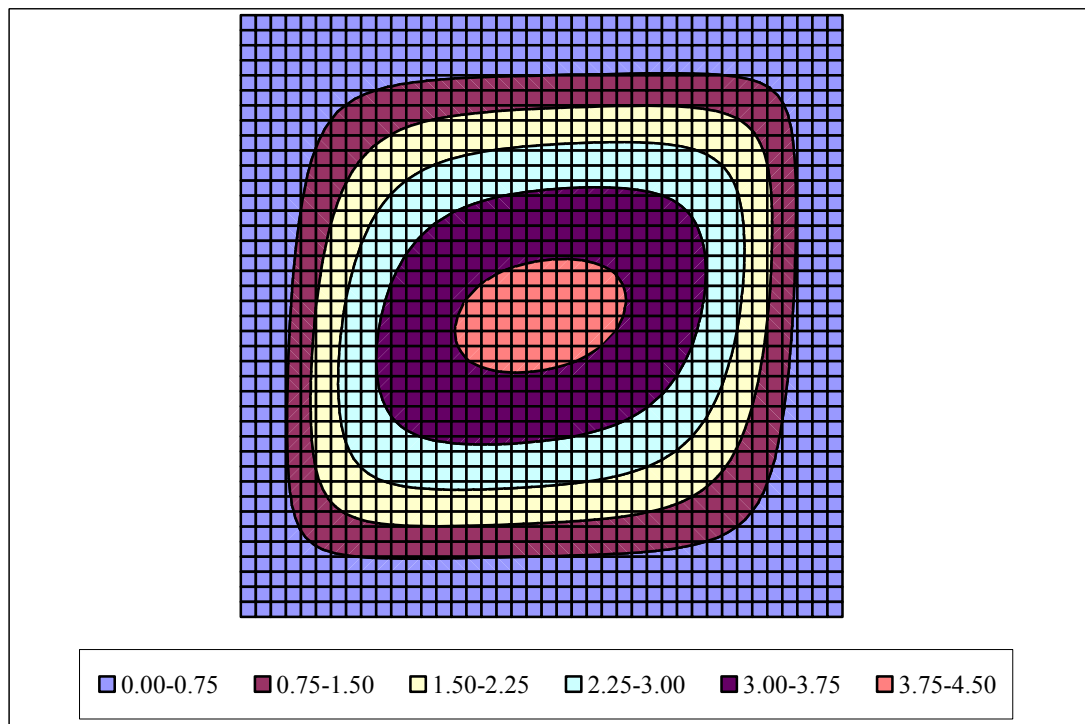**Figure 5.20:** Streamlines for Da=0.001, Ra$_H$=80, Pr=0.7, A=1, φ=0.5

| 0.00-0.25 | 0.25-0.50 | 0.50-0.75 | 0.75-1.00 | 1.00-1.25 | 1.25-1.50 |
| 1.50-1.75 | 1.75-2.00 | | | | |

Figure 5.21: Streamlines for Da=0.000001, Ra$_H$=20, Pr=0.7, A=1, φ=0.5

| 0.00-0.50 | 0.50-1.00 | 1.00-1.50 | 1.50-2.00 | 2.00-2.50 |
| 2.50-3.00 | 3.00-3.50 | | | |

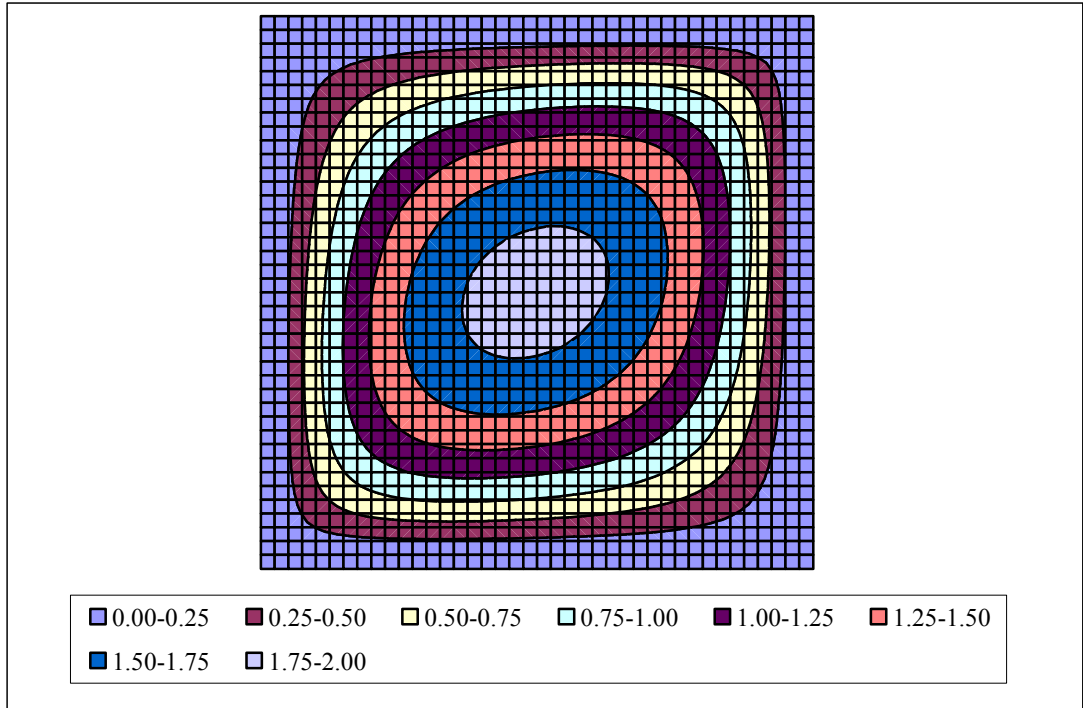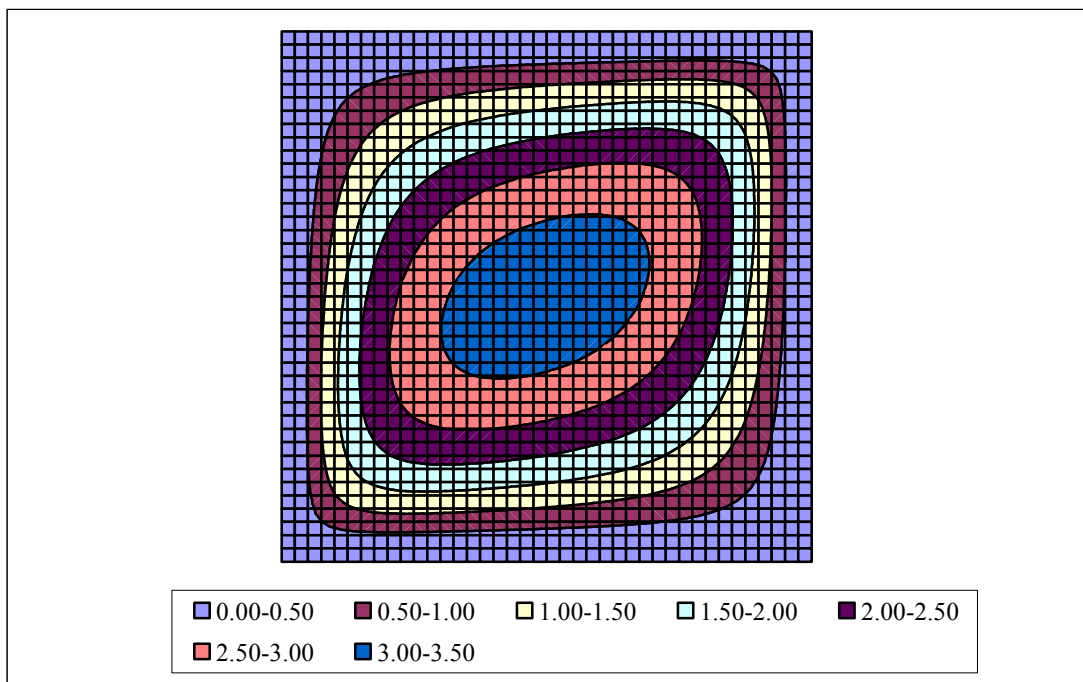**Figure 5.22:** Streamlines for Da=0.000001, Ra$_H$=40, Pr=0.7, A=1, φ=0.5

Figure 5.23: Streamlines for Da=0.000001, Ra$_H$=80, Pr=0.7, A=1, φ=0.5

5.4 Nusselt Number Values

Nusselt number is the ratio of convective heat transfer rate to that for pure conduction. In the absence of convection Nusselt number value approaches to unity, which will be explained in the upcoming sections. Using no-slip boundary conditions it is applicable to use the conduction heat transfer between nodes adjacent to the boundary where the natural convective heat transfer occurs from the boundary to the fluid. By applying the three point approximation for the finite difference method the Nusselt number values, the Nusselt numbers for the constant temperature side walls are as follows:

For the left hand side wall;

$$Nu = \frac{\int_0^H -k\left(\frac{\partial T}{\partial x}\right)_{x=0} dy \overset{\overbrace{}}{}^{heat-flux}}{\underbrace{kH\frac{\Delta T}{L}}_{conduction}} \cong \frac{A}{2\Delta T}\sum_{j=1}^{m}\frac{-3T_{1,j}+4T_{2,j}-T_{3,j}}{\Delta x}$$
(5.1.a)

and similarly the Nusselt number for the right hand side wall;

$$Nu = \frac{\int_0^H -k\left(\frac{\partial T}{\partial x}\right)_{x=L} dy \overset{\overbrace{}}{}^{heat-flux}}{\underbrace{kH\frac{\Delta T}{L}}_{conduction}} \cong \frac{A}{2\Delta T}\sum_{j=1}^{m}\frac{-3T_{n,j}+4T_{n-1,j}-T_{n-2,j}}{\Delta x}$$
(5.1.b)

There occurs small round off errors for the separate walls due to the iterative type of convergence in the program. To eliminate the effect of these minor errors the arithmetic average of these two Nusselt number values is used in the later sections which is:

$$Nu = \frac{A}{4\Delta T}\left[\sum_{j=1}^{m}\frac{-3T_{1,j}+4T_{2,j}-T_{3,j}}{\Delta x} + \sum_{j=1}^{m}\frac{-3T_{n,j}+4T_{n-1,j}-T_{n-2,j}}{\Delta x}\right]$$
(5.2)

5.4.1 The Effect of Darcy Number

While examining the effect of a specific constraint, all variables except the one whose sole effect will be under investigation are kept constant. For the Darcy number which is in the range of $10^{-8}<Da<10^{-1}$ the Rayleigh number based on height is also changing to have the effect of Rayleigh number on Nusselt number. Here the program is run for 6 different values of Rayleigh number and five different values of Darcy number. The results of these total runs are plotted in Figure 5.24. For all of these results the variables kept constant are $Pr_f=Pr_m=0.7$, $\varphi=0.5$, A=1.
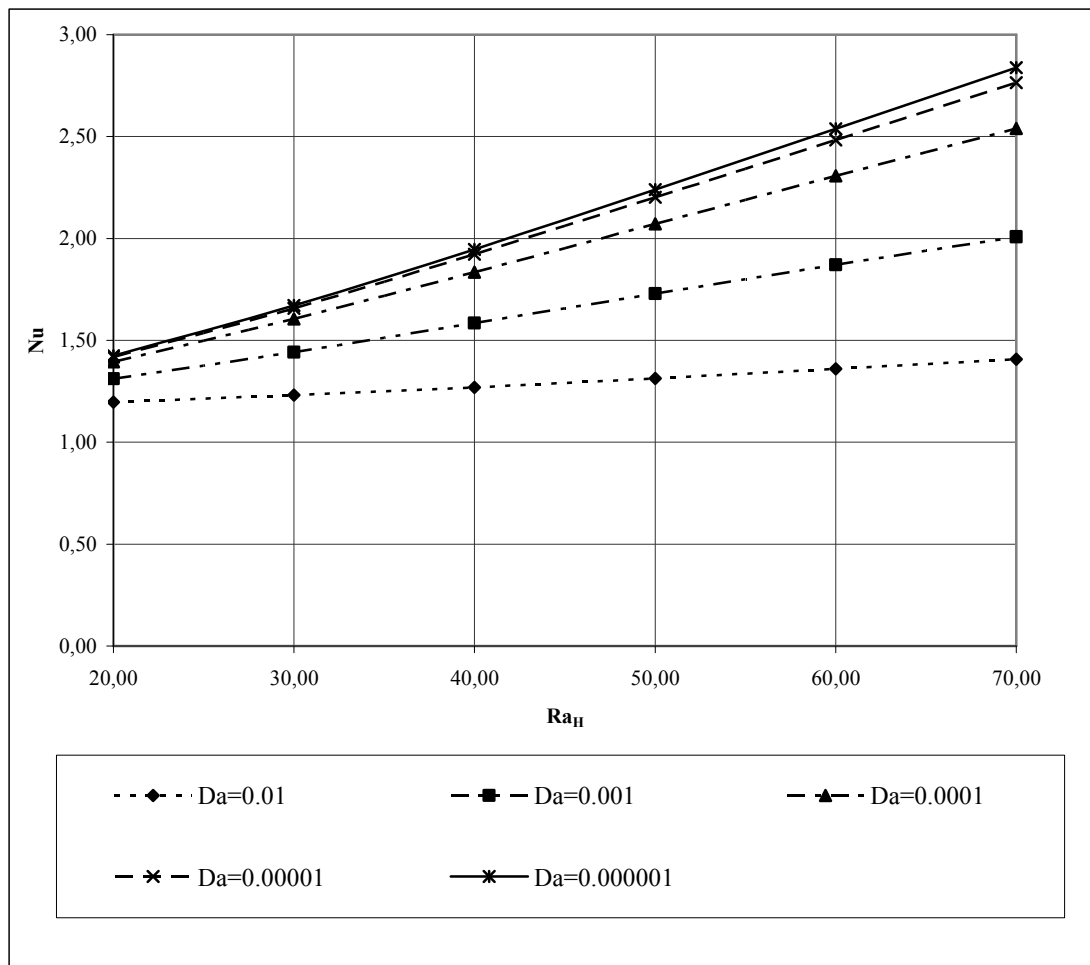
58

Figure 5.24: Variation of Nusselt number with Rayleigh number based on height for different values of Darcy number (where $Pr_f=Pr_m=0.7$, $\varphi=0.5$, $A=1$)

It can be seen from the figure that the Nusselt number is inversely proportional to the Darcy number. In other words, a decrease in the permeability will be followed by an increase in the total convective heat transfer through the medium. The effect of the Rayleigh number is more significant in the region $0.000001<Da<0.0001$. In the studies of Colburn with the packed tubes versus empty tubes, it was also stated that with higher Darcy numbers the sensitivity to change in Rayleigh number is negligible.

5.4.2 The Effect of Prandtl Number

The effect of Prandtl number on the Nusselt number (on the convective heat transfer) is investigated and examined for the equal Prandtl numbers of fluid and the medium.
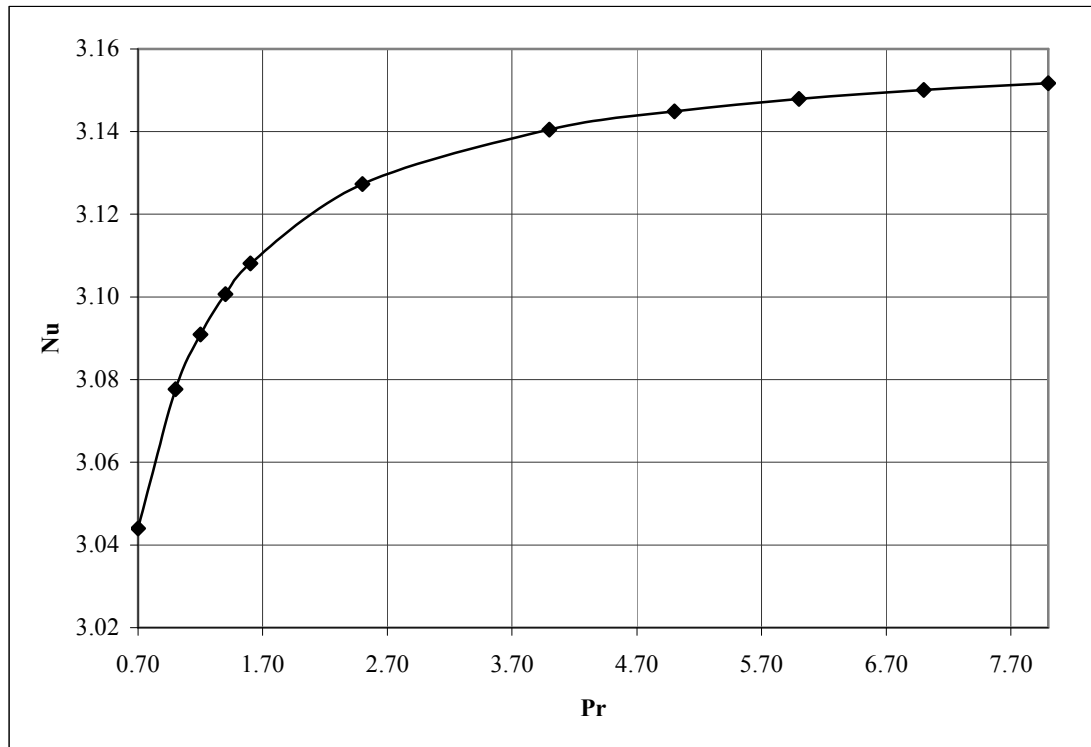
Figure 5.25: Variation of Nusselt number with Prandtl number (Da=0.00001, φ=0.5, A=1)

As seen from the figure in the range of 0.7<Pr<3.7 an increase in Prandtl number value results an increase in Nusselt number, whereas in the range of approximately 3.7<Pr<6.7 the relative change in Nusselt number with respect to the increase in the Prandtl number is very small. After Pr=7 the change in Nusselt number with the increase in Prandtl number is negligible.

5.4.3 The Effect of Conductivity Ratio

In this section the effect of conductivity ratio which is the ratio of Prandtl number of medium to the fluid is examined against the Nusselt number, while changing the Prandtl number of the fluid. This situation is demonstrated in Figure 5.26.
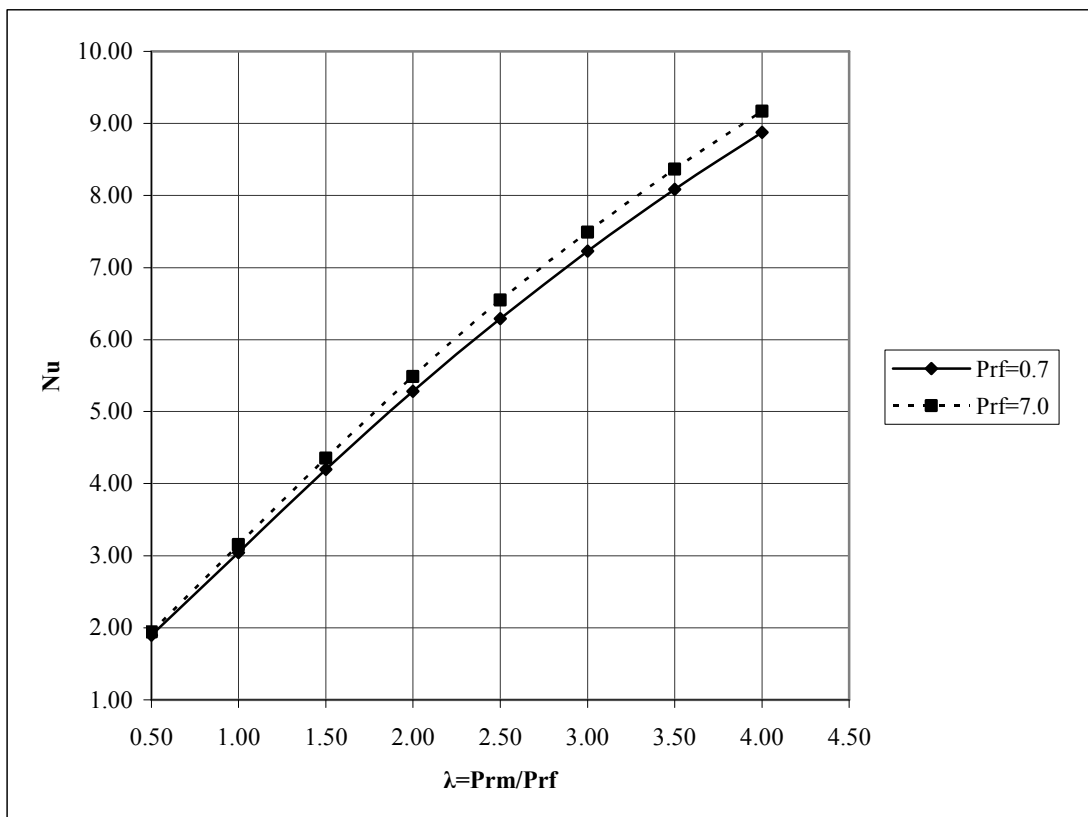

Figure 5.26: Variation of Nusselt number with the conductivity ratio for different Prandtl numbers (Da=0.00001, φ=0.5, A=1)

As seen from the Figure 5.26, Nusselt number is much more sensitive to the change in conductivity ratio, the ratio of Prandtl number of medium to that of the fluid, than to the change in Prandtl number of the fluid. There is a significant change

in the magnitude of the Nusselt number due to the change in the conductivity ratio. On the other hand, for $Pr_f=0.7$ and for $Pr_f=7.0$ Nusselt number values are very close for the same conductivity ratio.

5.4.4   The Effect of Porosity

When examining the effect of porosity on the Nusselt number, a wide range of porosity is used, $0.1<\varphi<0.99$. Moreover, two different conductivity ratios are used with the porosity. The above mentioned situation is shown in Figure 5.27.
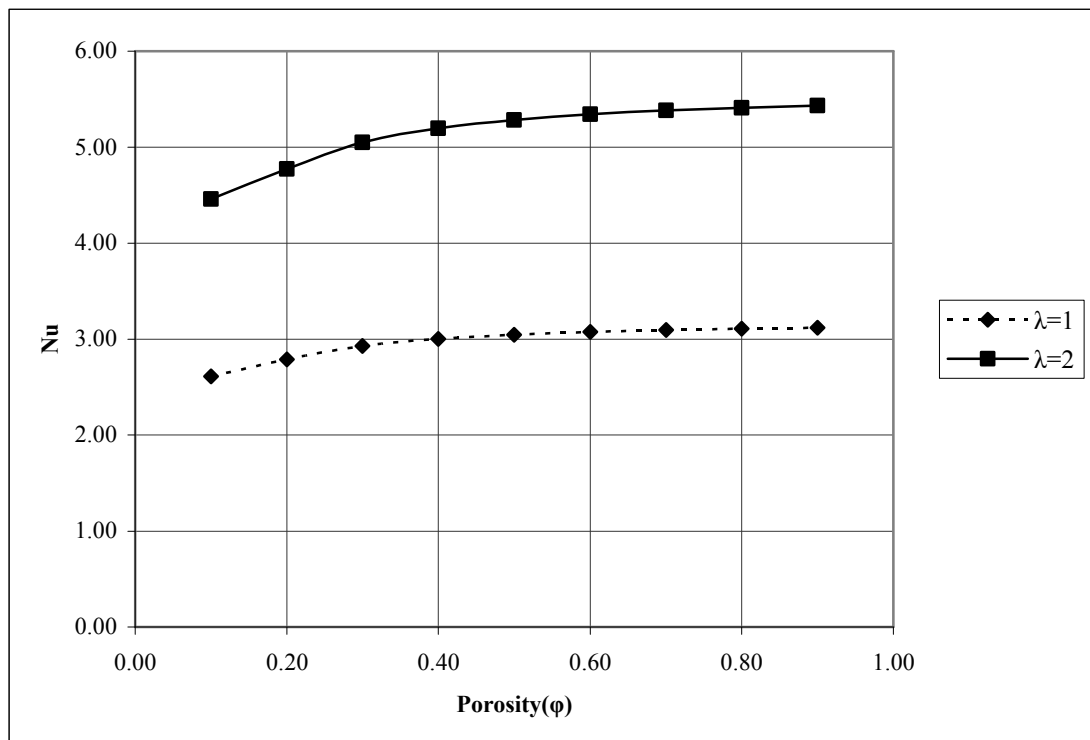

Figure 5.27: Variation of Nusselt number with Porosity for two different Conductivity Ratio Values (Da=0.00001, A=1)

The above demonstration shows that the effect of porosity becomes more significant when the conductivity ratio is relatively high. For λ=2 increase in Nusselt number is higher than the one with λ=1. Besides this result, it can be seen that the effect of porosity for both case is more obvious in the range of 0.1<φ<0.6. Beyond this Nusselt number is nearly unresponsive to any change in porosity.

5.5   Comparison of Results with Previously done Studies

In this section, the numerical results of the study will be compared and examined with respect to the previously done studies by various researchers.

The studies used here for the comparisons are; Weber's analytical solution and Bejan-Tien analytical solution.

Weber [26] developed an analytical solution for the boundary layer regime by applying the Oseen linearization method. As a result the total heat transfer rate between the two side walls can be expressed as the conduction referenced Nusselt number defined as the conductive heat transfer ratio and given by;

$$Nu = 0.577 \left(\frac{L}{H} \right)^{1/2} Ra_L^{1/2} \tag{5.3}$$

This situation then studied widely later by Bejan [27].

After Weber's study, Bejan and Tien reached an equation which is adequate for heat transfer calculations in tall layers at low and high Rayleigh numbers, and nearly identical to Weber's solution for high Rayleigh number regime.

$$Nu = 0.508 \left(\frac{L}{H} \right)^{1/2} Ra_L^{1/2} \tag{5.4}$$

Both Weber's and Bejan's studies are applicable for mediums of L/H<1 (tall mediums), and can not be applied for shallow mediums. On the other hand, the numerical solution presented in this study is applied for all aspect ratios i.e. $A \leq 1$ and $A \geq 1$.

The comparison table and graph are presented in Table 5.9 and Figure 5.28. It can be seen that the outcomes of the Fortran code comply with the other studies.

Table 5.9: Comparison of the Results with Previous Studies

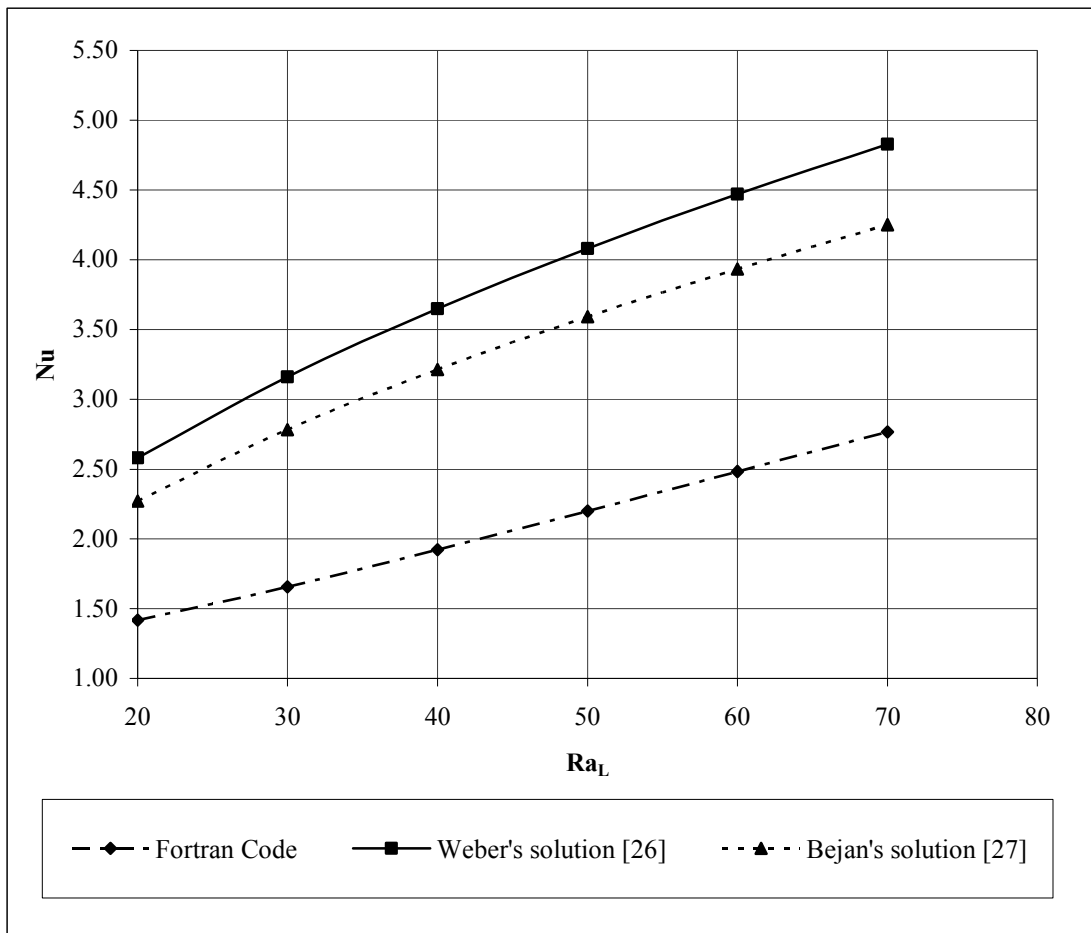| Ra_H	Numerical Solution	Weber's Solution	Bejan-Tien Solution
20	1.4185	2.5804	2.2718
30	1.6575	3.1604	2.7824
40	1.9232	3.6493	3.2129
50	2.2007	4.0800	3.5921
60	2.4826	4.4694	3.9350
70	2.7648	4.8275	4.2502

Figure 5.28: Comparison of the Results with Previous Studies, A=1

The numerical solution for A=1 is an acceptable match with Bejan's [27] and Weber's [26] solution. As a result the function that represents the curves should be similar. Thus, the function that represents the Nusselt number inside the porous medium will be as follows;

$$Nu = \alpha A^m Ra_L{}^n \qquad (5.5)$$

In order to find constants α, m and n, the Fortran code should be run for different cases. In order to find α and n Nusselt number values for aspect ratio of unity are plotted against Rayleigh number based on height.

The chart shows a curve with equation $y = 0.253x^{0.5355}$, plotting Nu against Ra_L, with legend items "Numerical Solution" and "Curve Fitting for Numerical Solution".
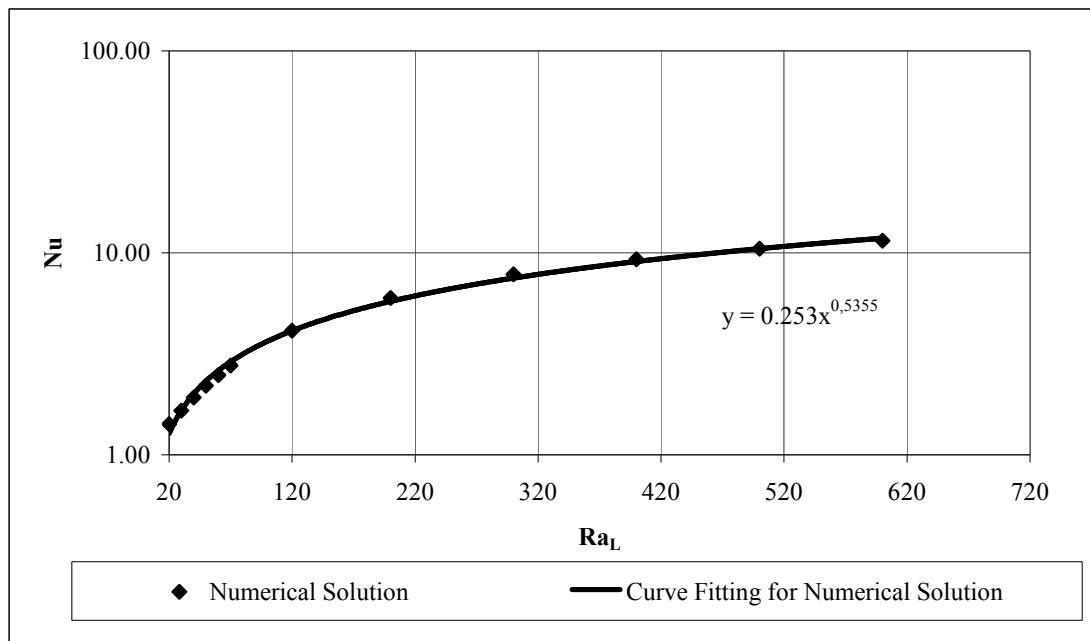
Figure 5.29: Nusselt number for different Rayleigh numbers, A=1

In Figure 5.29, A is the aspect ratio and Ra_L is the Rayleigh number based on horizontal distance from the origin of the porous medium. As can be seen from the graph, α and are determined through a curve fit tothe numerical solution for an aspect ratio of unity. For the remaining unknown quantity, m of Equation (5.5) different aspect ratios were used i.e. A=0.2-0.5-1-2-5.

65

The code as well as Equation (5.5) is applicable for 0.2<A<5. However, the resulting equations in the form of Equation 5.5 are different for aspect ratios greater than unity and for aspect ratios smaller than unity, which are as follows:

$$Nu = 0.253A^{0.225}Ra_L^{0.5355} \quad \text{for } 0.2<A<1 \tag{5.6.a}$$

$$Nu = 0.253A^{-0.213}Ra_L^{0.5355} \quad \text{for } 1<A<5 \tag{5.6.b}$$

Figure 5.30 is the demonstration of comparison of the study with previously done studies for A=0.5, i.e. a tall cavity. For shallow cavities Walker and Homsy [28] studied an asymptotically analysis and found the Nusselt number approximation as follows;

$$Nu = 1 + \frac{1}{120}Ra_L^2\left(\frac{1}{A}\right)^4 \tag{5.7}$$

Figure 5.31 is the comparison of the numerical solution with this mentioned equation for A=2, i.e. a shallow cavity. However Walker and Homsy [28] approach is mainly applicable for A>10 which is out of range of this study.

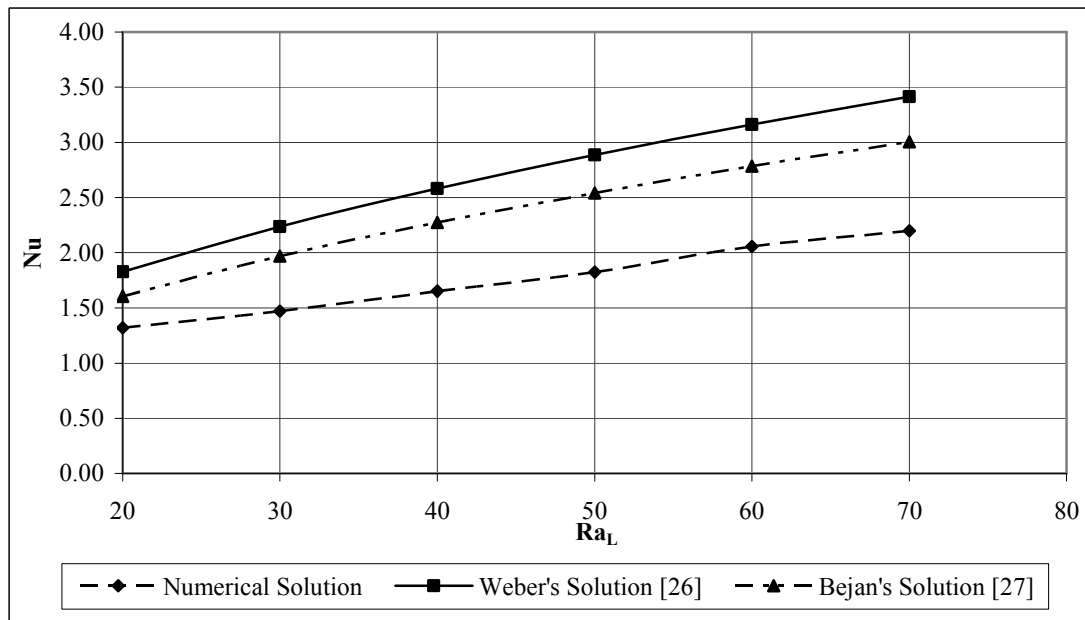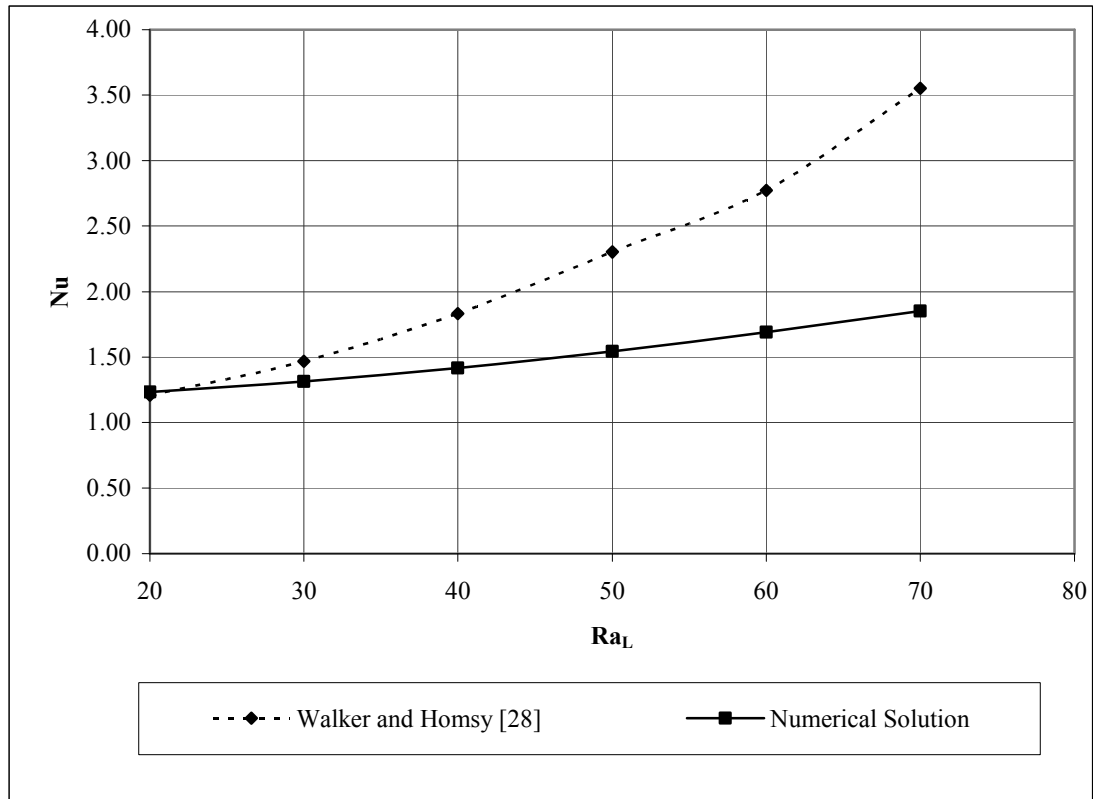**Figure 5.30:** Comparison of the Results with Previous Studies, A=0.5

Figure 5.31: Comparison of the Results with Previous Studies, A=2

5.6 Analysis of Heat Transfer Modes throughout the Medium for Different Aspect Ratios

As mentioned in the previous sections of the study, an aspect ratio is used for solving the finite difference equations. In the main program, where the results are shown an aspect ratio of one is used. In order to observe the change of the mode of heat transfer in the porous medium with saturated fluid inside, various aspect ratios are used. It can be seen from Figure 5.32, that for H/L values of order of magnitude of 0.1 and smaller or 10 or higher, Nusselt number value reaches almost unity and the mode of heat transfer is similar to conduction. So from the figure the heat transfer rate reaches a maximum when rectangular domain is nearly square when the Rayleigh number based on the height is fixed.

67
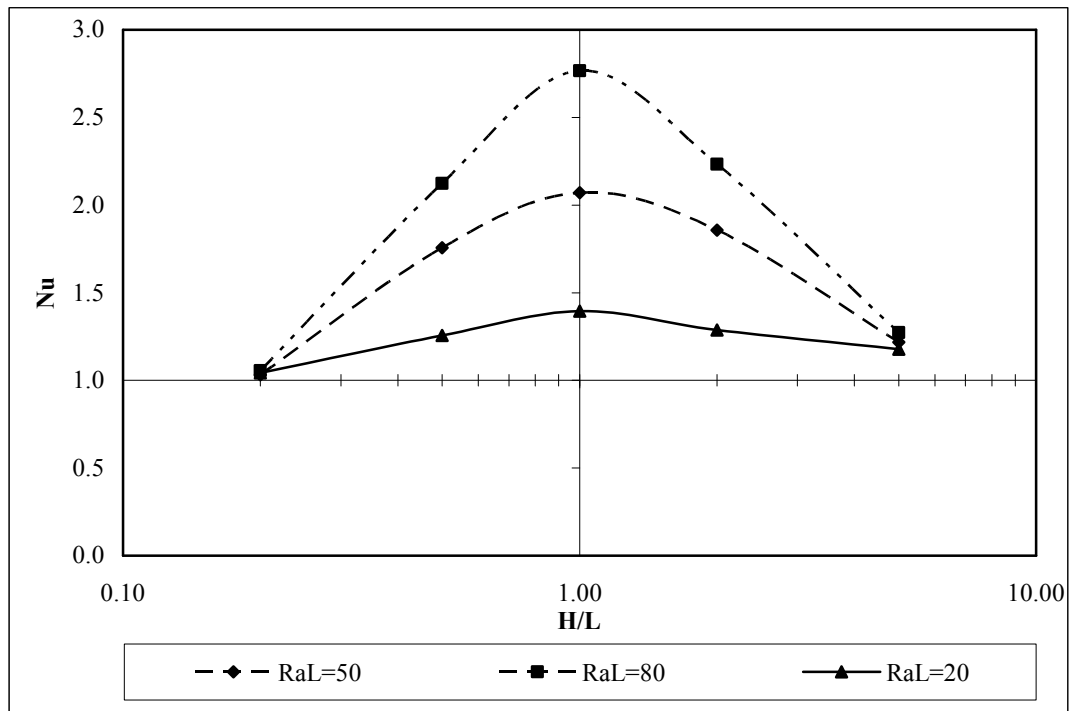
Figure 5.32: The effect of the height of the enclosure on the heat transfer rate (Nusselt number) (Da=0.00001, Pr=0.7, φ=0.5)

In Figure 5.32, Ra_L is the Rayleigh number based on the horizontal dimension of the porous medium. For aspect ratio of unity Ra_L is same with Ra_H.

The above stressed condition is well fit with the study of Bejan [29], in which he studied the optimization of heat transfer through a porous layer with saturated fluid inside and heated from the side. As stated previously, the numerical solution and the corresponding equations are applicable to both shallow and tall models within the pre-fixed regions.

CHAPTER 6

CONCLUSION

The studies on heat transfer through porous medium have recently increased because of worldwide concern with issues such as energy self-sufficiency and pollution of the environment. Insulation of buildings and equipments, energy storage and recovery, geothermal reservoir, nuclear waste disposal, chemical reactor engineering, the storage of heat-generating materials, and geothermal applications such as the flow of groundwater around hot intrusions are the main areas of applications of heat transfer through porous medium. Moreover, enclosures heated from the side are most representative of porous medium systems that function while oriented vertically, as in the insulations for buildings, industrial cold-storage installations and cryogenics.

Several studies have been done on the heat transfer through a porous medium up to now to predict the effect of the thermodynamics and environmental properties on the heat transfer rate. Some of them neglect the inertial forces some of them neglect the viscosity terms while deriving the basic equations of the control volume. In this study both terms are taken in to account for the rectangular control volume having the condition of heated from one side steady state steady flow through a porous medium. A FORTRAN based computer program is used to pick up the results for simulating the situation inside the porous medium.

The data collected from the simulation of the program is used to calculate the Nusselt number for the medium, as well as to examine the effects of most of the thermodynamic properties on the Nusselt number. For different values of Rayleigh, Prandtl and Darcy numbers Nusselt number graphs were plotted and followings

results were reached. The plotted graphs show that an increase in the Rayleigh number, will result an increase in the Nusselt number regardless of any change in Darcy number. However, the rate of this increase in the Nusselt number is dependent on the order of magnitude of Darcy number. As Darcy number decreases the Nusselt number values become more sensitive to the changes in Rayleigh number. The effect of Darcy number on isotherms and streamlines are presented in Chapter 5.

Other variables that affect Nusselt number are porosity and conductivity. Nusselt number is more sensitive on the change in conductivity ratio than the change in porosity, while it has a weak dependence on the porosity. On the other hand the change in the thermal conductivity values while keeping the conductivity ratio constant results almost no change in Nusselt number.

In Section 5.5 of the study, the results obtained from the generated Fortran code are compared with the previously done studies on heat transfer through porous medium. As stated in Chapter 5, there are several studies on calculating the total heat transfer through a fluid saturated porous medium subjected to end to end temperature difference. As a result of the numerical solution presented in this study a set of equations is presented to predict the heat transfer through the porous medium. For the tall systems (A<1) Weber's [26] and Bejan's [27] studies are presented and compared with the numerical solution presented in Chapter 5. The equation for tall layers generated from the numerical solution is appropriately fit with the previously done studies. For the shallow systems (A>1) the study of Walker and Homsy [28] is presented and compared with the numerical solution. The behavior of both equations are similar but there occurs slight difference in the order of magnitude of Nusselt number calculated from these equations. This difference is mainly due to the fact that Walker and Homsy's solution is widely applicable for higher aspect ratios.

As a last step for the study an analysis of aspect ratio versus Nusselt number is done. It is observed that Nusselt number that is the heat transfer through porous medium is maximum when the aspect ratio is unity for which the control volume is perfect square. Furthermore, from the plotted graph it is examined that the Nusselt number is sensitive to aspect ratio of 0.2<A<5. Beyond this range the change in

aspect ratio does not result any change in Nusselt number which becomes unity for aspect ratios of higher than 10 and also smaller than 0.1. So the Fortran code is said to be applicable in this aspect ratio. The range in which the code gives applicable results is as follows:

$$10 \leq Ra_L \leq 600$$
$$10^2 \leq Ra \leq 10^8$$
$$10^{-8} \leq Da \leq 10^{-1}$$
$$0.2 \leq A \leq 5$$

As the concluding remarks, the correlations mentioned in Chapter 5 are the main outcomes of the study. These equations well predicts the convective heat transfer behavior of the saturated porous medium. As stressed previously the previous studies [26, 27, 28] are limited to aspect ratios for $A \leq 1$ or $A \geq 1$. Whereas the below correlations that fits the numerical solution are well predicts the Nusselt number for both $A \leq 1$ or $A \geq 1$, but for a limited range of aspect ratio.

$$Nu = 0.253A^{0.225}Ra_L^{0.5355} \text{ for } 0.2 \leq A \leq 1 \qquad (5.6.a)$$

$$Nu = 0.253A^{-0.213}Ra_L^{0.5355} \text{ for } 1 \leq A \leq 5 \qquad (5.6.b)$$

The present study is for laminar flow regimes and a limited aspect ratio for the control volume. In future, the study may be improved in order to cover turbulent flow regimes and an increased range of aspect ratio. Different control volumes with different boundary conditions may also be studied for porous medium.

REFERENCES

1. Colburn, A.L., 1931. "Heat transfer and pressure drop in empty baffled and packed tubes", Ind. Eng. Chem., Vol.23, p. 910-923

2. Combarnous, M.A., and Bories, S.A., 1975. "Hydrothermal convection in saturated porous media", Adv. Hydrosci., Vol.10, p. 232

3. Darcy, H. P. G., 1856, "Les fontaines publiques de la ville de Dijon", Paris.

4. A. Hazen, 1893, "Some physical properties of sand and gravels with special reference to their use in filtration", Massachusetts State Board of Health, Twenty-fourth Annual Report, p. 541

5. Dullien, F. A. L., 1992, "Porous media: fluid transport and pore structure", 2nd ed. Academic Press, New York.

6. Kozeny, J., 1927, "Ueber grundwasserbewegung", Waseerkraft und Waseerwirtschaft 22, p. 67

7. Szekely, J. and Carr, R. G., 1968, "On nonisothermal flow of gases through packed beds", Transactions of the Metallurgical Society of AIME 242", p. 918-921

8. Ling, J. X. and Dybbs, A., 1992, "The effect of variable viscosity on forced convection over a flat plate submersed in a porous medium", ASME Journal of Heat Transfer 114, p. 1063-1065

9. Nield, D. A. and Lage J. L., 1997, "Convection effect on the porous medium flow of a fluid with temperature dependent viscosity", ASME Journal of Het Transfer

10. Whitaker, S., 1986, "Flow in porous media I: A theoretical derivation of Darcy's law", Transport in Porous Media 1, p. 3-25

11. Ene, H. I. and Polisevski, D., 1987, "Thermal flow in porous media", Reidel

12. Mei, C. C., Auriault, J. L. and Ng, C. O., 1996, "Some applications of the homogenization theory", Adv. Appl. Mech. 32, p. 278-348

13. Joseph, D. D., Nield, D. A. and Papanicolaou, G., 1982, "Nonlinear equation governing flow in a saturated porous medium", Water Resources Res. 18, p. 1049-1052

14. Joseph, D. D., Nield, D. A. and Papanicolaou, G., 1982, "Nonlinear equation governing flow in a saturated porous medium", Water Resources Res. 19, p. 591

15. Ward, J. C., 1964, "Turbulent flow in porous media", ASCE J. Hydraul. Div. 90, p. 1-12

16. Brinkman, H. C., 1947, "A calculation of the viscous force exerted by a flowing fluid on a dense swarm of particles", Appl. Sci. Res. A1, p. 27-34

17. Brinkman, H. C., 1947, "On the permeability of media consisting of closely packed porous particles", Appl. Sci. Res. A1, p. 81-86

18. Lundgren, T. S., 1972, "Slow flow through stationary random beds and suspensions of spheres", J. Fluid Mech. 51, p. 273-299

19. Vafai K. and Tien, C. L., 1984, "Boundary and inertia effects on fflow and heat transfer in porous media", Int. J. Heat Mass Transfer Vol.24, p. 195-203

20. Hsu, C. T. and Cheng, P., 1990, "Thermal dispersion in a porous medium", Int. J. Heat Mass Transfer 33, p. 1587-1597

21. Ergun, S., 1952, "Fluid flow through packed columns", Chem. Engng. Prog. 48, p. 89-94

22. Pepper, D.W. and Baker, A. J., 1988, "Finite differences versus finite elements", Handbook of Numerical Heat Transfer

23. Frankel, S.P., 1950, "Convergence rates of iterative treatments of partial differential equations", Math Tables and Other Aids to Computation, Vol. 4, p. 65-75

24. Young, D., 1954, "Iterative methods for solving partial differential equations of elliptic type", Trans. Am. Math. Soc., Vol. 76, p.92-111

25. Roache, P. J., 1976, "Computational fluid dynamics", Hermosa Publishers

26. Weber, J. E., 1975, "The boundary layer regime for convection in a vertical porous layer", International Journal of Heat Mass Transfer 18, p.5659-573

27. Bejan, A., 1984, "Convection heat transfer", Wiley, New York

28. Walker, K. L. and Homsy, G. M., 1978, "Convection in a porous cavity", Journal of Fluid Mechanics 87, p.449

29. Bejan, A., 1980, "A synthesis of analytical results for natural convection heat transfer across rectangular enclosures.", International Journal of Heat Mass Transfer 23, p.723-726

30. Bejan, A. and Nield, D. A., 1999, "Convection in porous media", Springer-Verlag New York, Inc.

31. Ingham, D. B., 2003, "Current issues on heat and mass transfer in porous media", NATO Advanced Study Institute on Porous Media.